DEGREE PROGRAMME IN WIRELESS COMMUNICATION ENGINEERING

MASTER'S THESIS

REFLECTION MEASUREMENT OF BUILDING MATERIALS AT MICROWAVES

Author Ankit Regmi

Supervisor Adj.Prof. Erkki Salonen

Second Examiner Dr. Markus Berg

Technical Supervisor Veikko Hovinen

January, 2016

Regmi A. (2016) Reflection Measurement of Building Materials at Microwaves. University of Oulu, Centre for Wireless Communication, Degree Programme in Wireless Communication Engineering. Master's Thesis, 78 p.

ABSTRACT

Radio waves interact differently with different materials. The knowledge of reflection and transmission characteristics of the electromagnetic waves through and from the building walls is the key in designing a radio propagation model. The dielectric properties of the material determine the behavior of reflection and transmission of the electromagnetic waves. Therefore, an oblique reflection model is implemented in this thesis to estimate the dielectric properties of various walls at frequency range of 0.7–7 GHz (6.3 GHz bandwidth). The measurement setup consists of a four-port vector network analyzer, two wideband dual-polarized cross-shaped Vivaldi antennas and two 8 m long coaxial cables. Measurements for parallel and perpendicular polarizations are achieved simultaneously by using the dual-polarized antennas. Time-domain gating is applied to separate the desired reflection and eliminate all other multiple reflections from the environment and to suppress the Line-of-Sight component from the delayed response.

The estimation of dielectric property of a material is an optimization problem where a suitable objective function is minimized to get the appropriate value. A theoretical model is implemented, so that the minimum difference between the theoretical and measured absolute value of reflection coefficient gives an estimated value of complex relative permittivity. The non-linear least squares algorithm is used for optimization purpose. The real and imaginary part of complex relative permittivity is investigated in this thesis. The real part signifies the amount of electric energy stored in a material, and is called dielectric constant whereas the imaginary part is called the loss factor, which signifies the dissipation of the radiated energy. The estimated values are in good agreement with the values found in the literature. The estimated dielectric properties in this study, such as dielectric constant, loss tangent and Brewster angle of the various materials can be utilized further in designing radio propagation models for similar environments.

Keywords: electromagnetic waves, complex relative permittivity, oblique incidence, Brewster angle, free-space measurements.

TABLE OF CONTENTS

FOREWORD

This thesis work has been carried out as a partial fulfilment for the completion of degree towards the Master's Degree Programme in Wireless Communication Engineering, at the Center for wireless Communication, University of Oulu, Finland.

I am grateful to my supervisors Erkki Salonen, Markus Berg, and Veikko Hovinen for supervising this thesis. Their support, comments, and reviews were crucial for the completion of the thesis. I would like especially to thank my technical supervisor Veikko Hovinen, for assisting me during all the measurements and looking into all technical aspects of the thesis. My warmest thanks go to my colleagues Bilal Khan, Zafar Hussain, Faisal Rehman, Lalit Ghimire, and Ashish Thapa for their support and motivation throughout the span of my thesis work.

This thesis is dedicated to my parents and sister for their unconditional love, encouragement, and support.

LIST OF ABBREVIATIONS AND SYMBOLS

AM	amplitude modulation
EM	electromagnetic
ECAL	electronic calibration
FNBW	first-null beamwidth
FFT	fast Fourier transform
HPBW	half-power beamwidth
IF	intermediate frequency
IFFT	inverse-fast Fourier transform
LHCP	left-hand circular polarization
LOS	line-of-sight
MUT	material under test
MSE	mean-squared error
PSO	particle swarm optimization
RHCP	right-hand circular polarization
TDR	time domain reflectometry
TRL	thru, reflect and line calibration
VNA	vector network analyzer
VSWR	voltage standing wave ratio
SWR	standing wave ratio
XPD	cross-polarization discrimination

$\mathbf{B}$	magnetic flux density
B	bandwidth
d	thickness of the wall
d_1	distance from antenna to the surface
d_2	distance from surface to the antenna
d_{LOS}	line-of-sight distance
d_{refl}	reflected distance from the wall
$d_{\mathrm{m\_refl}}$	reflected distance from metal floor
$\mathbf{D}$	electric flux density
D	largest dimension of the antenna
D	directivity
e_{c}	conduction efficiency
e_{d}	dielectric efficiency
e_{r}	reflection efficiency
e_{o}	total efficiency
$\mathbf{E}$	electric field strength
$\mathrm{E_i}$	incident electric field
$\mathrm{E_r}$	reflected electric field
f	frequency
$\mathrm{F}(\varepsilon_r)$	objective function
G	gain

G_{r}	receive antenna gain
G_{t}	transmit antenna gain
$\mathbf{H}$	magnetic field strength
$\mathbf{J}$	current density
k_{B}	Boltzmann's constant
N_f	number of frequency samples
N_θ	number of incident angles
P_{r}	received power
P_{N}	thermal noise power
P_{t}	transmitted power
r	distance away from the antenna
$s(t)$	signal in time domain
$S(f)$	signal in frequency domain
t	time
T	transmission coefficient
T	temperature
$w[n]$	Kaiser-Bessel window
Z_{in}	input impedance
Z_{o}	characteristic impedance
β	shape of the filter
δ	electrical thickness
ε^*	complex permittivity
ε_o	permittivity of free-space
ε_{r}	complex relative permittivity
$\varepsilon_{\mathrm{r}}'$	dielectric constant
$\varepsilon_{\mathrm{r}}''$	loss factor
λ	wavelength
μ	permeability
μ_o	permeability of free-space
μ_{r}	relative permeability of material
Γ	reflection coefficient
Γ_{meas}	measured reflection coefficient
$\Gamma_{\mathrm{tot\_thy}}$	theoretical reflection coefficient
θ_{b}	Brewster angle
θ_i	angle of incidence
θ_r	angle of reflection
θ_t	angle of transmission
$\tan\delta$	loss tangent

1. INTRODUCTION

Indoor wireless communications are one of the fastest growing sectors in this era of communication. Extensive development in radio communication systems has been witnessed over the past decades. Increasing demand for high performance and low-cost Personal Communication Systems has made the way for development of indoor radio communication systems. A key to design an efficient wireless network, in-depth knowledge of radio wave propagation in the radio channel is required.

Radio channel characterization is most important for system design and planning. The analysis of indoor coverage of radio signals is getting tougher with the changes in the environment and the variation of construction materials. Therefore, the building materials and their behavior with the electromagnetic waves have to be characterized before designing an indoor propagation model. The key parameters that are needed for material characterizations are the transmission and reflection properties of the propagating waves and their behavior, on interaction with various materials. Several microwave material characterization techniques have previously been used for predicting the behavior of radio signal in an indoor environment, such as dielectric waveguide technique, resonant cavity techniques, open-ended coaxial line technique and free-space technique. Out of the mentioned techniques, free-space and open-ended coaxial cable techniques are non-destructive whereas the rest are destructive techniques. Main drawback of waveguide technique is the requirement for the sample of the material to fit into the waveguide sample holder or cavity resonator. Whereas in a coaxial non-destructive approach the contact between the sample and probe is very critical, as a small gap or discontinuity can lead to significant errors. Therefore, a non-destructive free-space method was implemented for the reflection measurements at normal incidence and oblique incident angles. [1], [2]

A free-space reflection measurement technique was used for the measurement of electromagnetic properties of the building materials in a non-destructive setup. This thesis focuses mainly on the reflection of different building materials at microwave frequency band in different measurement setups. Extraction of samples of the material under test (MUT) was not possible in this case and the dielectric measurement cannot be made destructively. Therefore, a non-destructive procedure was required to characterize the layered material or sample [3]. Four different types of walls were selected for the measurement purpose.

Measurements was taken at 0.7–7 GHz (6.3 GHz bandwidth) using a vector network analyzer (VNA), and two wideband dual polarized cross-shaped Vivaldi antennas. Transmission parameters for both the parallel and perpendicular polarization were recorded, and the relative dielectric constant was estimated against theoretical results. Electronic calibration was applied according to the specifications of the VNA to achieve measurement with minimum error. Several sources of errors such as line-of-sight components and multiple reflections, diffraction from edges and scattered wave from rough surfaces, can affect the measurement data. These unwanted data can interfere with the measured reflection data and cause error. Therefore, time domain gating has been used to correctly determine the reflection peak and eliminate any other components from the response. A theoretical reflection model was used for the estimation of dielectric properties of various building materials. An algorithm was formed for the estimation of dielectric constant by fitting the theoretical reflection coefficient with the measured value. The measured and reflected values of reflection

coefficient were in good agreement with each other. The estimated values of dielectric permittivity of various walls were compared with previous results found in various literatures.

Several methods have been derived over the past few decades to extract the electromagnetic properties of various materials using reflection and transmission coefficients. Few of the important works done in this area are discussed in the next section.

1.1. Related Works

Over past few decades', a large amount of research has been done and different indoor radio propagation methods has been invented to characterize the electrical properties of building materials. Comparisons between these findings have assisted researchers to use the most efficient techniques for estimating the electromagnetic properties of building materials.

A free-space measurement of reflection and transmission coefficients for estimating the complex dielectric properties of a building wall has been carried out in [1]. Measurements were made from 2.4 GHz to 17 GHz frequency range using two orthogonal polarizations. A VNA was used for the measurement along with two horn antennas. Here estimation of complex dielectric constant is made using optimization. Reference [1] compares two methods for calculation of complex dielectric constant, namely the non-linear least square method and Particle Swarm Optimization (PSO). PSO was found to be a more efficient method as it yields smaller mean square error value. Parallel polarization shows smaller value of complex dielectric constant compared to perpendicular polarization.

In [3], open-ended coaxial probe method was used to measure the electromagnetic properties of hardened concrete specimen. Open-ended coaxial probe method was used because measurements are possible for wide range of microwave frequencies. Here, the measurement frequency range was from 0.1 GHz to 20 GHz. Concrete specimen were subjected to various settings of moisture that varied from oven dried samples to wet concrete. It was observed that, at dry conditions the dielectric constant shows similar behavior throughout the frequency range but in moist conditions, the dielectric constant varies significantly i.e. it increases rapidly with the increase in moisture content in the concrete specimen. The significance of the Brewster's angle was also studied. It was found that correct measurement of Brewster's angle of a specimen leads to improved detectability of certain target as the reflection from the target will be substantial as compared to the reflection from the concrete specimen.

Measurements involving construction materials for different types of buildings was performed in [4], and results were based on the received power over a range of frequency from 800 MHz – 18 GHz. Comparisons were made between various types of building, ranging from old building, office building to modern ones. The results suggest that attenuation of signal increases significantly in the modern buildings, as the new energy-efficient buildings are built with extra layers of building materials. Attenuation of 25 dB to 45 dB was observed in cold countries (Finland) where thick layers of construction materials are used for insulation. Old buildings gave lower values with the average attenuation of 10 dB throughout the frequency range. Thus, these measurements enable us to improve the radio propagation models for indoor-to-outdoor

communication, and to familiarize the nature of buildings and the level of expected attenuation.

Reference [5] has developed a free-space measurement system in a frequency range of 14.5 GHz to 17.5 GHz for measuring the dielectric properties of planar slab of ceramics and composite materials. Here, an algorithm has been developed that finds the zeros of the error function and calculates the dielectric constant using the reflection coefficients. Thru, reflect, and line (TRL) calibration technique was used to minimize the effects of multipath propagation. Two spot-focusing horn antennas were used to reduce the effect of diffraction from the edges of the samples. It has been shown that if the minimum transverse dimension of the sample is greater than three times the beam width of the antenna at the focus, the diffraction from the edges of the sample is insignificant.

The scope of this thesis is the estimation of dielectric properties of building materials using reflected fields at several incident angles. In references, [1,5-9], the measurement procedure using reflected and transmitted fields are used for the estimation of dielectric properties of various materials. However, they use different algorithms to solve the equations but the approach is common for all the methods. The estimation of dielectric constant in all cases is an optimization process in which a suitable objective function is minimized. The minimum error is calculated by the objective function between the theoretical and measure value of reflection coefficient for the estimated value of permittivity. Non-linear least square solver was used in this study to optimize the objective function. The same approach was used in references [6] and [8].

2. ANTENNA THEORY AND ELECTROMAGNETIC PROPAGATION

2.1. Antenna Fundamentals

Antennas are the most important element in wireless communication, as only the antennas have the capability to send or receive a signal wirelessly. Their dimensions vary from a few millimeters up to several meters depending on the application and frequency of operation. They can vary vastly in their shapes as well, i.e. there exists several types of antennas such as: wire antennas, aperture antennas, microstrip antennas, array antennas, reflector antennas, lens antennas, etc.

Antenna is a device which when excited by a suitable source can radiate or receive electromagnetic energy. It is a reciprocal device; if an antenna transmits with a particular radiation pattern and certain polarization, it has the capability to receive the similar mentioned radio waves [10]. Antennas are constructed using very good conducting metals such as copper, brass, aluminum, etc. When a time-varying current is accelerated (or decelerated) in the conducting metal, energy is dissipated in the form of radio waves. The transmission lines transport the radio waves from the source to the antenna. In case of perfect matching between the transmission line and the antenna, all the power will be delivered to the antenna i.e. no reflected power. The radiation can be manipulated by modifying various parameters of the antennas such as power, shape, size, orientation etc. The key parameters that describe the antenna are its directivity, gain, radiation pattern, radiation intensity, beam width, efficiency and polarization. [11]

2.1.1. Directivity, Gain and Efficiency

Directivity is the ability of the antenna to radiate maximum in a particular direction compared to other directions or receive maximum energy from a particular direction compared to other. According to [11], directivity is defined as the ratio of radiation intensity in a given direction to the radiation intensity averaged over all directions. In case of dual orthogonal polarization exists in the antenna, the total directivity of the antenna will be the sum of partial polarizations of both the polarization components [11]. The directivity of an isotropic antenna is unity. If an antenna has a narrow main beam, the directivity will be higher whereas in case of wide main beam, the directivity will be lower [12].

Gain is another parameter that highlights the capability of the antenna, and it is very closely related to directivity. The gain takes into account both the efficiency and the directivity of the antenna. Thus, gain is considered as a practical value of directivity and is given by the following equation:

$$G = e_o D, \tag{2.1}$$

where e_o is the total efficiency and D is the directivity of the antenna. [11]

The total efficiency of an antenna takes into account all the losses in the antenna, such as reflection losses, dielectric and conduction losses etc. Therefore, combining reflection, dielectric and conduction efficiencies, one can determine the total efficiency

of an antenna. Reflection efficiency is the measure of impedance mismatch between the transmission line and the antenna as some of the power is reflected back due to mismatch degrading the performance of the antenna. The conduction and dielectric efficiencies are the measures of the losses that occur due to the material used for construction of the transmission line and the antenna. Thus, the total efficiency is given by:

$$e_o = e_r e_c e_d, \tag{2.2}$$

where e_r, e_c, e_d are reflection, conduction and dielectric efficiencies, respectively.

2.1.2. Impedance Matching

If the characteristic impedance of the transmission line does not match that of the antenna, mismatch occurs i.e. some of the power delivered to the antenna will reflect back. The reflected signal and the input signal superimpose and give rise to a standing wave. Standing wave ratio (SWR), also called voltage standing wave ratio (VSWR) is the function of the reflection coefficient or insertion loss. Voltage reflection coefficient is defined as ratio of the reflected voltage to the forward voltage. Thus, VSWR is given by

$$\text{VSWR} = \frac{1 + |\Gamma|}{1 - |\Gamma|} \tag{2.3}$$

$$\Gamma = \frac{Z_{in} - Z_O}{Z_{in} + Z_O} \tag{2.4}$$

where Γ is the reflection coefficient that denotes the reflected voltage or insertion loss, Z_{in} is the input impedance of the antenna and Z_O is the characteristic impedance. If no reflection occurs then all the power is delivered to the antenna, and the impedance is considered to be matched. Thus, in this case the VSWR will be unity. The higher the value of VSWR, more is the degraded performance of the antenna. [13]

2.1.3. Beamwidth

Beamwidth is the angular separation of the main beam (maximum beam in a direction) measured from the common point originating at equal but opposite side of the beam. The main parameters regarding beamwidth are the Half-Power Beamwidth (HPBW) and First-Null beamwidth (FNBW). HPBW is the angle where the radiation intensity has half power compared to the maximum power of the beam. It is also called 3 dB beamwidth, as half power is 3 dB below the maximum. The angular separation between the first nulls of the radiation pattern is referred to as FNBW. The beamwidth can be used to target a region or to have coverage over the required region of interest. Hence, beamwidth and directivity are closely related as they describe the focusing ability of the antenna radiation pattern. [11,12]

2.1.4. Radiation Pattern

Radiation pattern is the graphical representation of the pattern of EM waves radiated by the antenna in the far field region. The variation of the power radiated by the antenna can be analyzed by its radiation pattern. The region around the antenna is divided in three parts, which are reactive near-field, radiating near field and radiating far field. The reactive near field of an antenna is the closest region to the antenna, here the reactive fields are more dominant compared to the radiating field. Radiation pattern cannot be visualized in the near field. The radiation pattern changes with distance travelled in the radiating near field, this region is also known as Fresnel region. The farthest region, where the radiation pattern of an antenna is defined is the far field region of the antenna, also known as Fraunhofer region. Radiation pattern is independent with increase in distance in this region and the field decreases as 1/r. The criterion for the antenna to be in the far field region is given by the following equation:

$$r > \frac{2D^2}{\lambda} \tag{2.5}$$

where r is the distance away from the antenna, D is the largest dimension of the antenna measured perpendicular to the direction of the radiated wave and λ is the wavelength. In the far field region, radiated waves behave as plane waves. [10,11]

2.2. Wave Propagation

Electromagnetic waves are the backbone of the wireless communication systems. Since, the discovery of electromagnetic waves in the 19th century, rapid advances in development of wireless communication technologies has kept going on. The study of wave propagation is necessary to analyze and design any indoor or outdoor propagation model.

Electromagnetic waves are generated by varying electric and magnetic fields excited by a suitable source. They can carry information via guided media such as transmission lines or coaxial cables or via free-space from one antenna to the other. The behavior of electromagnetic (EM) waves with other materials is defined by the Maxwell's equations. The four quantities around which the Maxwell equations are derived, are: electric flux density **D**, magnetic field strength **H**, electric field strength vector **E** and magnetic flux density **B**. The Maxwell's equations in differential form are presented as:

$$\nabla \cdot \mathbf{D} = \rho \tag{2.6}$$

$$\nabla \cdot \mathbf{B} = 0 \tag{2.7}$$

$$\nabla \times \mathbf{E} = -\frac{\partial \mathbf{B}}{\partial t} \tag{2.8}$$

$$\nabla \times \mathbf{H} = \mathbf{J} + \frac{\partial \mathbf{D}}{\partial t} \tag{2.9}$$

Equation (2.6), (2.8) and (2.9) represent Gauss' law, Faraday's law and Ampere's law with Maxwell's addition respectively. The relation between field strengths and flux densities bounded to some media can be given by their electric and magnetic properties as:

$$\mathbf{D} = \varepsilon \mathbf{E} \tag{2.10}$$

$$\mathbf{B} = \mu \mathbf{H} \tag{2.11}$$

where ε is the permittivity and μ is the permeability of the medium. [10, 14,15]

When electromagnetic waves travel from the transmit antenna to receive antenna through free-space, the attenuation of the power density decreases by $1/r^2$. This decreasing factor does not take into account the atmospheric conditions and irregularities of the system. Thus, the received power at the receiver in free-space is given by the Friis free-space equation:

$$P_r = P_t G_t G_r \left(\frac{\lambda}{4\pi r}\right)^2 \tag{2.12}$$

where P_r is the received power, P_t is the transmitted power, G_t is the transmitter gain, G_r is the receiver gain, λ is the wavelength, r is distance from transmitter to the receiver. The transmitted power will always be less than the power supplied to the transmit antenna and will always be greater than the received power. Similarly, the received power will always be less than power supplied to the receiving antenna. This is all due to losses in the system, which are caused by impedance mismatch, polarization mismatch, orientation of the antennas (if antennas are focused at incorrect angle), multipath fading, scattering, reflections etc. [10]

The attenuation of EM waves mainly depends on the frequency of the radiated wave. At very low frequencies, large antennas are required to transmit and usually they are ground-based vertical towers. This is because an antenna cannot be much shorter than a quarter wavelength to radiate with high efficiency. Therefore, simple antennas with low gain and more transmit power is used for low frequency transmission such as AM broadcast (0.55 to 1.6 MHz). At these frequencies, propagation takes place via ground and the phenomenon is known as surface wave propagation. The attenuation of surface waves increases with the increase in frequency, therefore for higher frequency or at microwave frequencies (300 MHZ to 30 GHz) transmissions, direct line-of-sight (LOS) or reflections from different surfaces is considered. At microwave frequencies, there is less atmospheric noise, therefore these are more suitable for broadcast than low frequency. [14]

2.3. Polarization

Electromagnetic plane waves consist of time-varying electric and magnetic fields that are perpendicular to each other, and perpendicular to the direction of propagation. In a practical communication system, the electric field vector of the plane wave travelling in z-direction can have both components, *x* and *y*, which can oscillate independently depending on the nature of the source generating the electromagnetic (EM) wave. Depending on the orientation of the electric field vectors, the behavior of the EM waves can be determined, and this behavior is defined as the polarization of the wave [16]. Thus, polarization of the wave determines the orientation of electric field vector that lie

in the plane perpendicular to the direction of propagation. It can be defined as that property of EM wave that describes the time varying direction and relative magnitude of electric field vectors, as observed along the direction of propagation [11]. Polarization can be classified as linear, circular and elliptical polarization.

Polarization of the antenna can be defined as the polarization of the waves radiated by the antenna. The polarization of the receiving antenna should be same as that of the arriving wave to receive maximum power. In case of different polarizations of receiving and transmitting antennas, most of the power is lost and less power will be received. This condition is called polarization mismatch and the power loss in this case is called polarization loss [11]. The term co-polarization is used when the receiving antenna has the same polarization as the wave incident on it. Whereas, cross-polarization represents that the polarization is orthogonal with respect to the specified polarization, hence maximum power loss is observed due to cross polarization effects. The behavior of electromagnetic wave is affected as they come in contact with a dielectric media. Parameters such as wavelength, power, and polarization are affected. This is due to the different values of relative permittivity and permeability of the dielectric materials. The classification of different polarizations are done below.

2.3.1. Linear Polarization

In plane wave propagation, both the electric and magnetic fields oscillate as transverse waves, i.e. the oscillation is perpendicular to the waves' direction of travel. When the oscillation is in a single direction, the plane is called linearly polarized. When the plane wave meets a boundary of two mediums with different electrical properties, two orthogonal field components are defined for calculating the interaction with the boundary. A parallel field component oscillates in the plane of incidence determined by the normal vector of the surface and by the direction vector of the propagation. The perpendicular field component is orthogonal to the parallel one. [11]

2.3.2. Circular Polarization

Circular polarization is achieved as a sum of two orthogonally polarized fields having equal magnitudes and relative phase shift of $\pi/2$. Circularly polarized wave is rotating along the direction of propagation, hence the name circular polarization [11]. The tip of the total electric field along the direction of propagation moves along a fixed circle as time progresses. If the electric field of the circularly polarized wave is rotating in counter-clockwise direction, the polarized wave is called *Right-hand Circular Polarization* (RHCP). It follows the right-hand thumb rule where the thumb is pointing in the direction of propagation whereas the fingers are curled in the direction of rotation of electric field. Similarly, if the rotation of electric field follows the left-hand thumb rule, or the electric field is rotating in clockwise direction, the wave is known as *Left-hand Circular Polarization* (LHCP) [16].

2.3.3. Elliptical Polarization

In a general case, any polarization state can be divided in two orthogonally polarized electric field components. Elliptical polarization is attained when the phase difference

between the components is $\pi/2$ but the magnitudes differ, hence forming an ellipse along the direction of propagation. Elliptical polarization is also attained when the time-phase difference between the two components are not an odd multiple of $\pi/2$, irrespective of their magnitude. [11]

2.4. Reflection and Transmission of EM Waves at different Interfaces

The extensive use of wireless technology has led to comprehensive study of radio wave propagation in several different environments. In largely populated urban area with tall buildings and complex building indoor structures, design of wireless communication system has to take into account a number of propagation effects. Propagation does not depend only on the direct LOS, as the waves will come across various obstacles from buildings and building walls that are constructed using various materials. Thus, propagation is explained by various mechanisms such as diffraction, reflection, transmission and refraction. Further, the EM fields change when they interact with various materials, as different materials possess different electrical and magnetic properties. The electric and magnetic properties of the materials are defined by their permittivity and permeability, respectively.

2.4.1. Complex Permittivity

The amount of electric energy stored in medium is defined by the permittivity and the ability of the material to form magnetic field is defined by its permeability. Absolute permeability is defined by relative permeability as $\mu = \mu_r \mu_o$, where the permeability of vacuum is $\mu_o = 4\pi \times 10^7$ H/m. Here, we only focus on non-magnetic materials, whose relative permeability is close to unity. Therefore, only permittivity will be discussed in detail.

Different materials have different EM properties and interact differently with the EM waves. Generally, all the materials that interact with the radiated waves in the present wireless communication systems are dielectric in nature. The electromagnetic waves change their properties such as wavelength, attenuation and wave impedance when they come in contact with a dielectric medium. This is mainly due to the difference in the relative permittivity and permeability (for magnetic materials) of two different media. The complex permittivity is given by [3]:

$$\varepsilon^* = \varepsilon_o \varepsilon_r \tag{2.13}$$

where ε_o is the permittivity of free-space = 8.845× 10^{-12} F/m and ε_r is the complex relative permittivity of the material and is given by:

$$\varepsilon_r = \varepsilon_r' - j\varepsilon_r'' \tag{2.14}$$

where ε_r' is the real part of complex relative permittivity and is known as the dielectric constant that signifies the amount of electric energy stored in the material. ε_r'' is the imaginary part of complex relative permittivity describing how lossy a medium is, or how much radiated energy is dissipated by the medium, and is also known as 'loss factor'. Loss factor for a lossless medium is zero and relative permittivity is real in this

case. Loss factor is usually much smaller than the dielectric constant. Dielectric constant for most materials is generally greater than 1. Dielectric constant of a material is not actually a constant and is dependent on frequency, nature of material, temperature, and humidity.

Loss tangent is another important parameter concerning the dielectric properties of a material. It is the ratio of energy lost to the energy stored in a material and is defined by the following equation.

$$\tan\delta = \frac{\varepsilon_r^{"}}{\varepsilon_r^{'}} \tag{2.15}$$

where tanδ is the loss tangent. The vector diagram for tangent loss in shown in Figure 1 [17].

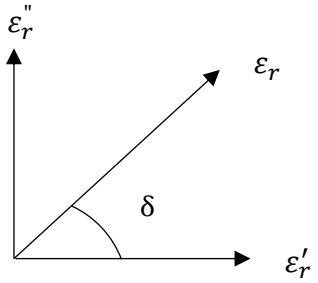

Figure 1. Loss Tangent Vector Diagram

2.4.2. Oblique Incidence of EM waves on Dielectric Interface

The study of oblique incidence of EM waves at dielectric surfaces helps in understanding the behavior of wave and their behavior at different polarizations. Figure 2 shows, a plane wave incident at an angle θ_i on a dielectric boundary [13].

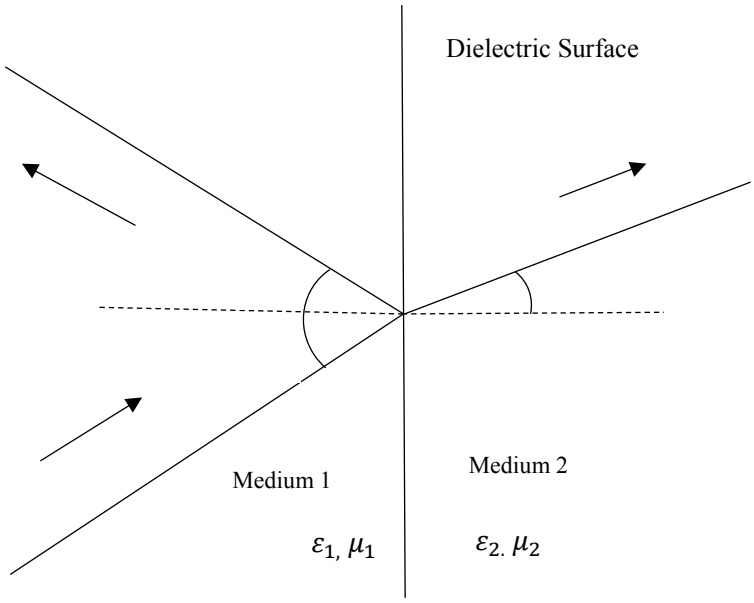

Figure 2: Plane wave incident on the dielectric boundary.

It is observed that some part of electric field incident on the dielectric boundary is reflected back to the same medium (Medium 1) and some part is transmitted or refracted into Medium 2. The wavelength of electromagnetic wave decreases when the wave is travelling from medium 1 to medium 2 and $\varepsilon_2 > \varepsilon_1$ and vice-versa. The angle of reflection θ_r can be determined using the Snell's law of reflection, given by:

$$\sin\theta_i = \sin\theta_r \tag{2.16}$$

$$\theta_i = \theta_r \tag{2.17}$$

It states that the angle of reflection at the boundary is equal to the angle of incidence. The polarization of the EM waves is independent of Snell's law of reflection [16]. For the transmitted wave, the angle of refraction (or angle of transmission) is the function of permittivity of the medium and is given by Snell's law of refraction derived by matching boundary conditions in [16]:

$$\sqrt{\varepsilon_1}\sin\theta_i = \sqrt{\varepsilon_2}\sin\theta_t \tag{2.18}$$

2.4.3. Reflection and Transmission Coefficient

Relation between the incident, transmitted and reflected electric field is given by the reflection and transmission coefficients. The reflection coefficient is a function of incident angle, propagation constant, frequency of radio waves, thickness of the medium, the complex permittivity of the medium and the polarization of the wave. When considering a free-space measurement system, the total reflected field can be considered as the superposition of infinite reflected fields from several layers of the

medium [2]. Thus, the total reflected field can be represented as an infinite geometric series as:

$$\begin{aligned} \mathrm{E_r} = \ & \Gamma_{12}.\mathrm{E_i} + \mathrm{T_{12}}\Gamma_{21}e^{-j2\delta}\mathrm{T_{21}}.\mathrm{E_i} \\ & + \mathrm{T_{12}}\Gamma_{21}e^{-j2\delta}\left(\Gamma_{21}^2e^{-j2\delta}\right)\mathrm{T_{21}}.\mathrm{E_i} \\ & + \mathrm{T_{12}}\Gamma_{21}e^{-j2\delta}\left(\Gamma_{21}^2e^{-j2\delta}\right)^2\mathrm{T_{21}}.\mathrm{E_i} \\ & + \cdots \end{aligned} \tag{2.19}$$

where, $\Gamma_{12}\ (=-\Gamma_{21})$, and $\mathrm{T_{12}}\ (=-\mathrm{T_{21}})$ are the reflection and transmission coefficient from medium 1 (air) to medium 2 (the wall), respectively, and $\Gamma_{21}, \mathrm{T_{21}}$ are the reflection and transmission coefficient from medium 2 to medium 1, respectively. [2]
The total reflection coefficient is given by the ratio of electric field reflected from the layered the dielectric medium to the electric field of the incident wave [1]. Thus, equation (2.19) takes the compact form as [2]:

$$\Gamma(\omega) = \frac{\mathrm{E_r}}{\mathrm{E_i}} = \frac{1-e^{-j2\delta}}{1-\Gamma_o^2e^{-j2\delta}}\Gamma_o \tag{2.20}$$

where δ is the electrical length and is given by the following equation:

$$\delta = \frac{2\pi d}{\lambda}\sqrt{\varepsilon_r - \sin^2\theta_i} \tag{2.21}$$

where d is the thickness of the medium, λ is the wavelength, and Γ_o is the Fresnel reflection coefficient, which is the reflection coefficient for either parallel or perpendicular polarization and is given by following equations, respectively [16]:

$$\Gamma_\perp = \frac{\cos\theta_i - \sqrt{(\varepsilon_2/\varepsilon_1) - \sin^2\theta_i}}{\cos\theta_i + \sqrt{(\varepsilon_2/\varepsilon_1) - \sin^2\theta_i}} \tag{2.22}$$

$$\Gamma_\parallel = \frac{-\varepsilon_2\cos\theta_i + \varepsilon_1\sqrt{(\varepsilon_2/\varepsilon_1) - \sin^2\theta_i}}{\varepsilon_2\cos\theta_i + \varepsilon_1\sqrt{(\varepsilon_2/\varepsilon_1) - \sin^2\theta_i}} \tag{2.23}$$

The total reflection coefficient is different for different polarizations. The Fresnel reflection coefficients are calculated applying boundary conditions with respect to the incident angle. An example of the behavior of reflection coefficient as a function of incident angles for both polarizations for $\varepsilon_r = 3 - 0.15\mathrm{i}$ and $\varepsilon_r = 6 - 0.15\mathrm{i}$, are shown in Figure 3 and Figure 4 respectively. Figure 3 and 4 are calculated using equations (2.20-2.23) The simulations were carried out at 6.3 GHz frequency for angle of incidence from 0 to 90 degrees. The thickness of 0.2 m was considered for the simulation. The minimum value to total reflection coefficient in Figure 3 is close to zero. The real part of complex permittivity dictates the location of Brewster's angle as can be seen from Figure 3; greater the dielectric constant larger is the Brewster's angle. Thus, for lossless materials, permittivity is a real quantity and the reflection coefficient becomes zero at the Brewster's angle for parallel polarization. The imaginary part of

permittivity clarifies the fluctuations in the reflection coefficient response, as it is a function of losses in a material.

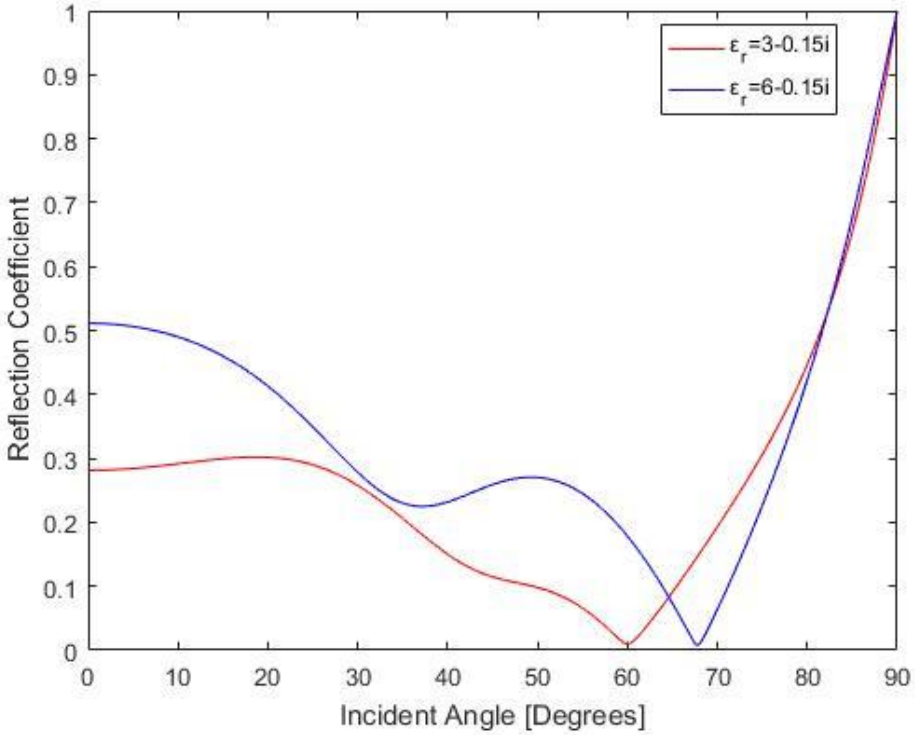

Figure 3: Reflection Coefficient (Parallel Polarization)

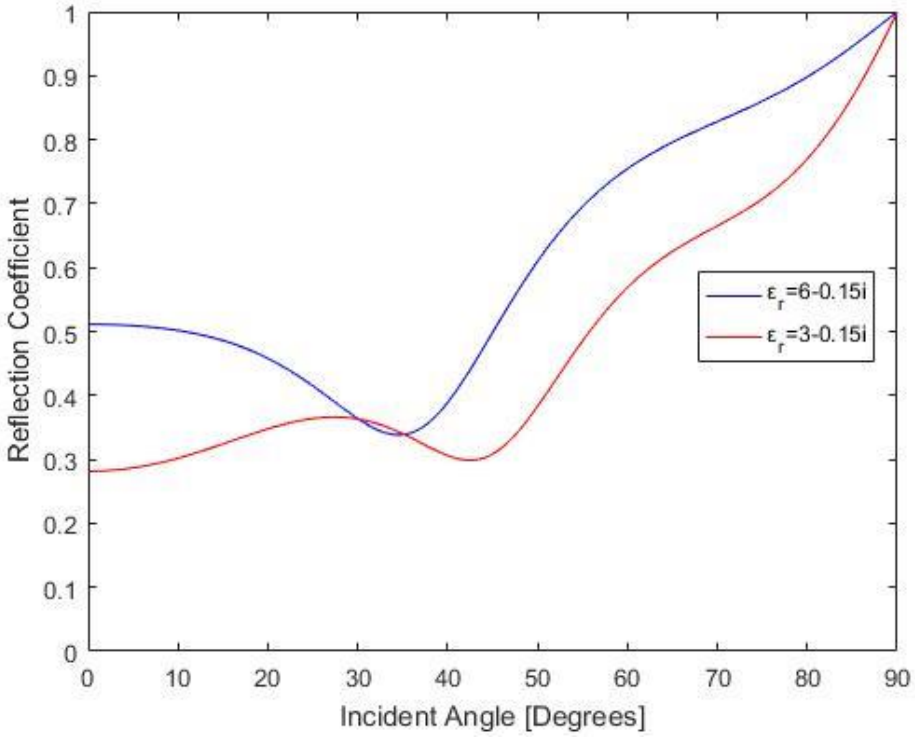

Figure 4: Reflection Coefficient (Perpendicular Polarization)

The transmission coefficient for normal incidence i.e. $\theta_i = 0^o$ is given by [16]:

$$T_\perp = 1 + \Gamma_\perp \text{ and } T_\parallel = (1 + \Gamma_\parallel)(\cos\theta_i / \cos\theta_t) \tag{2.24}$$

whereas for oblique incidence (i.e. $\theta_i \neq 0^o$) we have [16]:

$$T_\perp = \frac{2\cos\theta_i}{\cos\theta_i + \sqrt{(\varepsilon_2/\varepsilon_1) - \sin^2\theta_i}} \tag{2.25}$$

$$T_\parallel = \frac{2\sqrt{(\varepsilon_1/\varepsilon_2)}\cos\theta_i}{\cos\theta_i + \sqrt{(\varepsilon_1/\varepsilon_2)}\sqrt{1 - (\varepsilon_1/\varepsilon_2)\sin^2\theta_i}} \tag{2.26}$$

If the wave is incident on a perfect conductor, the wave is reflected back and the absolute value of reflection coefficient will be 1, whereas equations (2.20) to (2.23) will be valid for all the other cases.

2.4.4. Brewster's Angle

When the incident EM wave has parallel polarization, at some angle, the incident wave will be completely transmitted to the other medium. Thus, no reflection occurs i.e. $R_\parallel = 0$ (total transmission). The angle where the incident wave is totally transmitted, is known as Brewster's angle. It is a case of special angle of incidence [16]. Brewster's angle θ_b depends on the dielectric properties of the medium, and is given by [3]:

$$\theta_b = \tan^{-1}\sqrt{\frac{\varepsilon_2}{\varepsilon_1}} \tag{2.27}$$

Brewster's angle only exists in case of parallel polarization. When an arbitrary wave is incident at the Brewster's angle, only the perpendicularly polarized wave is reflected whereas the parallelly polarized wave is totally transmitted. Thus, in case of perpendicular polarization there is always some reflected waves. There can exist Brewster angles for both of the polarizations, if the mediums have different permeabilities. In this study, permeabilities for both mediums are considered the same (i.e. $\mu_r = 1$). Any arbitrarily polarized wave will be linearly polarized after reflection at Brewster's angle. This is also sometimes referred as 'Polarizing Angle' [18]. Brewster's angle can be described in another way as well, i.e. when the angle between the reflected wave and the transmitted wave become perpendicular to each other, at this point the angle of incidence will be equal to the Brewster's angle [16].

3. MICROWAVE MEASUREMENTS

Design of any propagation system requires precise evaluation of the entire environment. Therefore, efficient measurement systems are required to measure several parameters that account for the design of the communication system. In modern communication systems, we rely on various propagation mechanisms for efficient communication between the transmitter and the receiver such as: reflection from various surfaces, diffraction from the edges and refraction through the interface. The major indoor communication systems at present and in the future will be operating at microwave frequency range and above (millimeter wave region). Therefore, several microwave measurement techniques have been developed to measure and analyze various factors necessary for designing an efficient propagation model. The scope of this study focuses mainly on the reflections from building materials at microwave frequencies. The data collected will be valuable to analyze various parameters such as dielectric properties of the building materials at microwave frequencies, the Brewster's angle, total received power, multipath propagation along the path of propagation etc.

All measurement systems for inspecting material properties rely on the measurement equipment to collect the measured data. Measurement systems require a device that has the ability to store the output responses, and to display the results based on some standard parameter. A transmitter and a receiver are required to send and receive the signal, antennas or transmission lines can be used for this purpose, and the sample of the MUT is required whose properties are of the point of interest.

In this chapter, the measurement system and measurement methods are discussed in detail along with some important parameters that are the part of the functionality of the device used for the measurements.

3.1. Vector Network Analyzer

Measurements at lower frequencies can be done using simple tools such as a sine wave generator, a voltage meter, a current meter and a calculator. As the complexity of the communication systems has increased, so has the frequency of operation. Therefore, more complex measurement devices are needed for these calculations. Measurement of various parameters, such as impedance or reflection coefficient of active and passive high frequency devices, is very tedious using the traditional devices. Modern VNAs are designed to solve and perform complex calculations of active and passive high frequency devices. A VNA is a device capable of evaluating circuit responses based the signal fed into the network. A VNA also stores the responses and display them on the instrument screen. It is a rather complex device capable of performing complex mathematical calculations based on the responses of the network. Thus, VNA characterizes these devices under test by measuring their network parameters such as, the scattering parameters (S-parameters). Therefore, a network analyzer is the only device that can measure the properties of materials, components, various circuits and systems accurately at microwave frequency. [19, 20]

VNA has the ability perform multiple measurements from a single connection. Measurements at RF and microwave frequencies are made fairly simple by the VNA. The basic structure of VNA consists of a source, signal separation devices and detectors [20]. The characteristics of the incident wave, reflected wave and the transmitted wave

can be easily analyzed by pressing a button on the VNA. These properties are displayed in the form of S-parameters, as the function of frequency and the extracted S-parameters can be converted manually to the required parameter via mathematical analysis. VNA is able to measure the amplitude and phase of the waves. Modern VNAs can display the measurements in both the domains i.e. in the time domain and frequency domain. The differences between the time and frequency domain measurements will be highlighted in section 3.1.2. Wide range of error in the system is removed by the calibration of the VNA. Calibration gives better accuracy and better rejection of broadband noise.

3.1.1. Scattering Parameters

Scattering parameters gives the relation between the incident, reflected and transmitted waves, as a function of frequency. Measurement or extraction of S-parameters of a network is the most accurate way of finding the characteristics of the electrical network such as impedance, attenuation, dielectric properties, VSWR, etc. They are generally represented in frequency domain. They are very important for the ease of design of the microwave systems. S-parameters can be extracted for any number of ports of a network.

S-parameters are presented as complex numbers, as both magnitude and phase of the incident wave are changed by the network [21]. S-parameters are represented in a matrix called scattering matrix. A simple 2-port network and the 2-port scattering matrix are shown in Figure 5, which defines the S-parameter precisely.

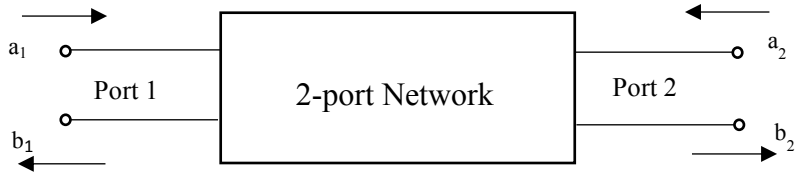

$$\begin{bmatrix} S_{11} & S_{12} \\ S_{21} & S_{22} \end{bmatrix}$$

Figure 5: Two-Port Network and its scattering matrix.

In Figure 5, a_1 and a_2 are the input signals at port 1 and port 2, respectively whereas b_1 and b_2 are the outgoing signals. The parameters 'a' and 'b' can be voltage or current or power travelling from port 1 to port 2 and they describe the outgoing and incoming characteristics of the signals or waves [20]. Thus, the S-parameters can be defined with respect to the relationship between these incoming and outgoing signals as follows:

$$[b] = [S][a] \tag{3.1}$$

$$b_1 = S_{11}a_1 + S_{12}a_2 \tag{3.2}$$

$$b_2 = S_{21}a_1 + S_{22}a_2 \tag{3.3}$$

Here, subindices i and j in S_{ij} represent, the destination port and the source port, respectively. Therefore, S_{11} signifies signal from port 1 coming back to port 1, and similarly we can derive this relationship for the remaining S-parameters [20].

$$S_{ii} = \frac{b_i}{a_i} \tag{3.4}$$

$$S_{ij} = \frac{b_i}{a_j} \tag{3.5}$$

Equation (3.4), gives the relations of the incident and the reflected wave, it is derived when the input signal applied at port i and the other port is terminated to a matching load or vice-versa, thus, b_j is totally absorbed which makes $a_j = 0$. Thus, S_{ii} and S_{jj} is also known as return loss or reflection coefficient. Similarly, equation (3.5), gives the relation between incident and transmitted waves and is derived when port i is the source port and port j is terminated to the matching load and vice-versa, which makes $a_i = 0$ and gives the relation in equation (3.5), which is known as insertion loss or transmission coefficient. Similarly, S-parameters can be derived for N-port networks. The scattering matrix for N-port is given below:

$$\begin{bmatrix} S_{11} & \cdots & S_{1\mathrm{N}} \\ \vdots & \ddots & \vdots \\ S_{\mathrm{N}1} & \cdots & S_{\mathrm{NN}} \end{bmatrix}$$

In this study, a 4-port VNA is used for the measurement. Thus, 4×4 S-parameter matrix is obtained, with each S-parameter containing two parts, amplitude and phase. This study is the case of oblique incidence, thus the term reflection coefficient here signifies, the ratio of the signal reflected from the dielectric boundary to the signal incident on the dielectric surface. Hence, the S-parameter of interest are horizontally polarized wave travelling from port 1 to port 2 i.e. S_{21} and vertically polarized wave travelling from port 3 to port 4 i.e. S_{43}.

3.1.2. Frequency Domain and Time Domain Measurements

A VNA measures the properties of a material, circuit or component and displays the result as S-parameters, in frequency domain. Previously, Time Domain Reflectometry (TDR) was used for time domain measurements and was done by observing the impulse response of the MUT on an oscilloscope [22]. The advances in the design of network analyzers have made it possible to visualize the measurements in the time domain as well. In VNA, time domain measurements are achieved by applying Inverse Fast Fourier Transform (IFFT) to the frequency domain signal. Time domain is the analysis that shows the change in data as impulse responses in terms of time differences, i.e. delays, or propagation distances. Frequency domain shows the data in terms of transfer functions, i.e. how much of the signal lies within each frequency over a range of

frequencies. In this study, the VNA was used directly to perform the conversion from frequency domain to time domain. In general, the relationship between the time-variant delay-spread function (='impulse response') and the time-variant transfer function can be given by the following relation [23]:

$$s(t,\tau) = \int_{-\infty}^{\infty} S(t,f).e^{j2\pi ft}\, df \tag{3.6}$$

$$S(t,f) = \int_{-\infty}^{\infty} s(t,\tau).e^{j2\pi ft}\, d\tau \tag{3.7}$$

where $S(t,f)$ and $s(t,\tau)$ are in this study the S-parameters in frequency and delay domains respectively. In the case of material measurements, the functions are not time-variant, i.e. they are only functions of delay τ and frequency *f*. Moreover, in this study, the delay-spread function $s(\tau)$ is said to be in 'time domain' to be consistent with the TDR terminology.

VNA operates with discrete frequency samples equally spaced over the measurement frequency, whereas in the above equations (3.6) and (3.7) the Fourier or inverse Fourier transform operates on the continuous data [22]. Thus, the transform applied does not give the exact conversion of the original signal as there are some discontinuities present in the converted signal that are not present in the original signal, which is mainly due to the energy leakage from one frequency to another. Therefore, windowing is applied to suppress these unwanted discontinuities in the original signal. The VNA uses IFFT with a suitable window function to convert from frequency domain to time domain. The VNA used for this study, uses a Kaiser-Bessel window for this purpose.

Windowing is a function, which is zero-valued outside the given interval. The purpose of applying a window function (or windowing) to the signal is to minimize the effects of the discontinuities in the original signal. Thus, windowing suppresses the components outside the given interval and highlights the region of interest. Windowing can be understood as the multiplication of the original signal with the window function of finite length, giving finite length version of the original signal [24]. A main lobe and many side lobes are observed after applying window function. The main lobe is the signal of point of interest and the side lobes are the lower amplitude signals or unwanted components of the signals. The efficiency of a window depends on the magnitude of the side lobes. The lower the magnitude of the side lobes as compared to the main lobe, the better is the efficiency of the window. The side lobe magnitudes arise due to the leakage from the window and the type of window used. The attenuation of side lobes and the width of the main lobe are inversely proportional to each other. The narrower the main lobe, the better is the frequency resolution of the window. Thus, there is a trade-off between the amplitude of the side lobes and width of the main lobe.

In this study, the VNA uses Kaiser-Bessel window and defined by the following Bessel's functions [25]:

$$w[n] = \begin{cases} I_o[\beta\left(1 - \left[\frac{n-\alpha}{\alpha}\right]^2\right)^{\frac{1}{2}}], & 0 \le n \le M \\ 0, & \text{otherwise} \end{cases} \tag{3.8}$$

where β is the parameter that determines the shape of the filter, M is the window length and controls the main lobe, α is equal to $M/2$. Here, β controls the main lobe width and the side lobe magnitude. As β increases, the magnitude of the sidelobes decreases and the width of the main lobe increases. Thus, suitable value of β will enable the good frequency resolution and significant side lobe attenuation at the same time. The VNA used for this study uses a consistent β value of 6 [22]. Figure 6 shows the behavior of the Kaiser window with different values of β, which are 0, 3, 6. As it can be observed from Figure 6 (right), the main lobe width increases and the sidelobe magnitude decreases significantly, as β increases from 0 to 6. The relative side lobe attenuation increases from -13.3 dB for $\beta = 0$ to -44.1 dB for $\beta = 6$ [22]. MATLAB was used to simulate the following responses of the Kaiser window with MATLAB's built-in function, 'Kaiser' and windows visualization tool was used to plot Figure 6.

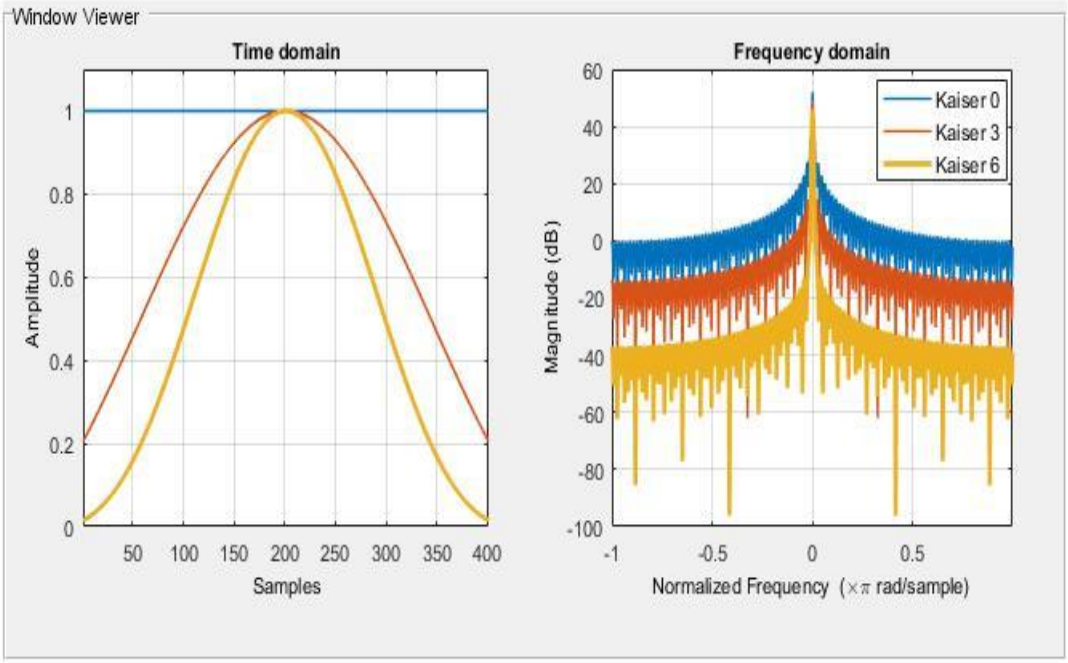

Figure 6: Kaiser Window with different β values

Time domain representation has some advantages over frequency domain. Time domain measurements help in finding the discontinuities in the components or the MUT. Any irregularities or faults in the measurement setup can be easily analyzed in time domain, as the function of delay or propagation distance. In a microwave measurement system, it is very simple to analyze all the multiple reflections and diffractions via different edges in time domain. Hence, time domain measurement is a more detailed representation of the behavior of the signal with the MUT, as the irregularities or the region of interest can be easily analyzed and separated out through 'gating', which will be discussed in detail in next section. The frequency domain representation only shows the response of the system (or MUT) for different frequencies. Therefore, direct visualization of irregularities or discontinuities cannot be achieved in frequency domain representation. But, due to higher dynamic range of frequency domain, lower instantaneous bandwidth is required as compared to time domain. Thus, error models are designed in frequency domain, and therefore less systematic errors occur due to better calibration in frequency domain. Hence, both time domain and frequency domain are the two different ways to look at the same system and

they are interchangeable parameters, i.e. no information is lost in changing from one domain to another.

In this study, the measurements were performed by the VNA in the frequency domain, but firstly, data measured in frequency domain were transformed to time domain to differentiate between the main reflection from the wall, direct LOS, diffraction and unwanted multiple reflections. This transformation was done manually by selecting the transform function in the VNA. Both the frequency and time domain data were collected for further analysis. An example for frequency domain vs time domain plot is shown in Figure 7. As observed, it is difficult to interpret the behavior of multiple reflections or other effects in the frequency domain plots, and the reflections from environment create additional ripples in the frequency domain. In the time domain plot, two significant peaks can be observed out of which one of the peak is the point of interest. Thus, time domain gating is applied to select the interested response, as shown and explained in the next section.

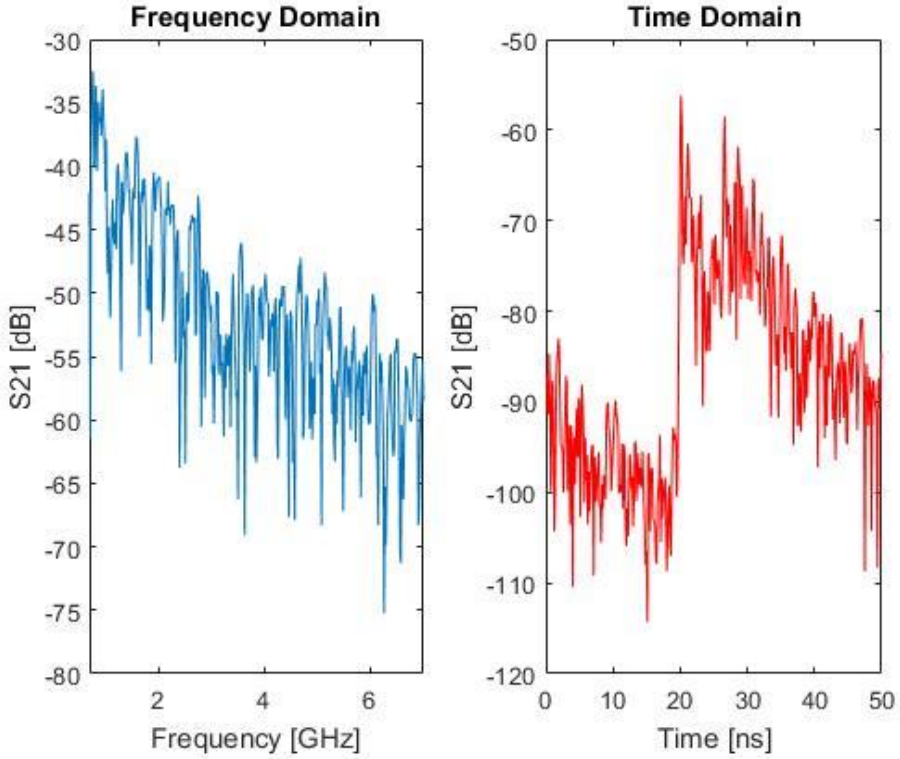

Figure 7: Frequency domain (left) Vs Time domain (right)

3.1.3. Gating

The measurement data may contain various unwanted information from the environment, or some unexpected fault in the measuring components. These faults can be visualized in time domain. Thus, these unwanted data can be filtered out and only the required data of interest can be extracted using gating. Hence, gating is the method to extract the response of interest. It is generally known as time domain gating. The gated signal can be converted to frequency domain using Fourier transform. A time domain gate is defined by a start and stop delays (or gate center and span) that determine the width of the gate (or gate interval). The part with the applied gate interval is observed,

and the part outside the gate interval is attenuated. The essential signal being observed is known as the main lobe and the attenuated signal outside the gate interval are called side lobes. Thus, it is important to notice that for effective gating, difference between the magnitude of the main lobe and the side lobes is significant. For example, a free-space measurement system will have many components arriving from the surroundings such as multiple reflections, LOS components, and diffracting signals having significant effect on the total received signal. If these components are present at different delays, they can be separated by time domain gating, and only the signal of point of interest remains. Figure 8, gives the clear insight to the current scenario. Time domain gating is applied to the measured responses of Figure 7 and shown in Figure 8. Only the point of interest is visible, i.e. the main reflection peak and other effects from the surroundings are attenuated significantly. It has to be noted that gating here is not applied in frequency domain, but the gated time domain signal is converted to frequency domain using Fourier transform. Gating was applied here with the span of 1ns.

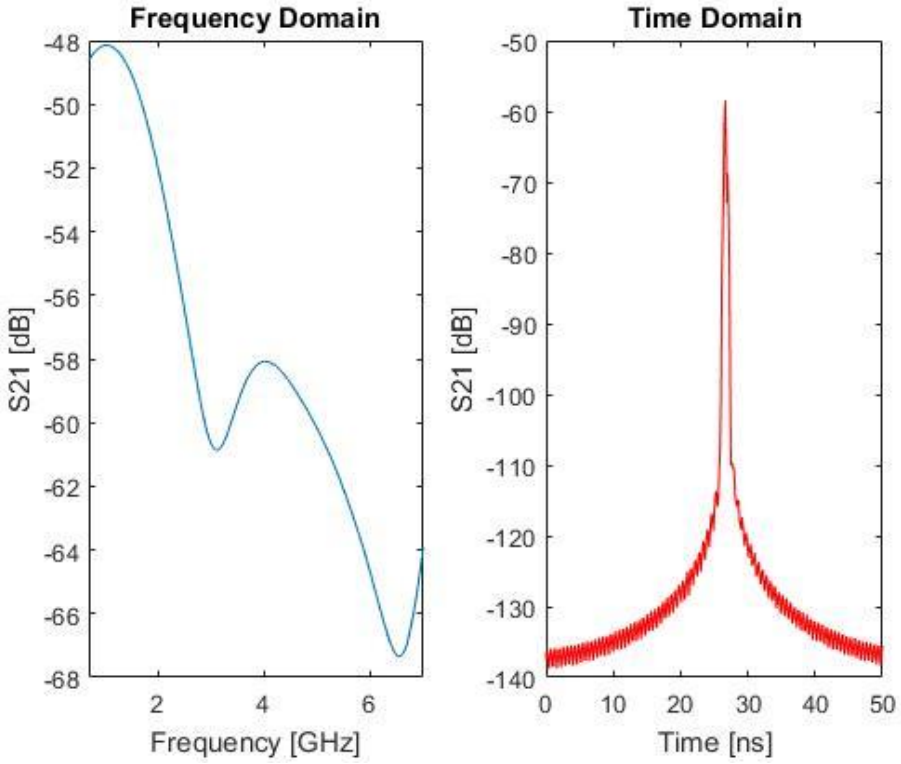

Figure 8: Gated Frequency Vs Gated Time

Thus, a gate is a kind of filter that has a passband ripple, a cut-off rate and side lobe level and the passband can be determined by the gate center and span [22]. Hence, applying a gating function to a signal gives the smooth response neglecting all the unwanted responses as can be seen in Figure 5.

3.1.4. Measurement Errors

Errors in the measurement can be caused by various measurements equipment's inaccuracies or due to the harsh environments. Thus, these errors in the measurement data can lead to catastrophic results, which can further bring a flaw in the design of the

system based on this erroneous measurement. Therefore, it is necessary to minimize the inaccuracies as much as possible by calibrating the instrument before the measurement. Calibration is the process of removing unwanted effects or errors from the connectors, cables connected to the measurement system. It sets a defined standard value for the components, comparing their current response to the response of the ideal model. Thus, calibration is done in order to enhance the measurement accuracy. In the case of VNA, calibration also sets a reference power level to zero dB, and sets the zero delay at the point of calibration, i.e. at the ends of the RF cables. There are several types of error sources introduced in the VNA, such as: drift errors, random errors, systematic errors, and monitoring error terms [18].

Drift errors are caused after the calibration has been done due temperature variations, which leads to thermal expansion of the connectors and cables within the instrument [18]. Therefore, measurement should be done in stable temperature conditions in order to minimize drift errors. Hence, recalibration is the way of minimizing these errors. Systematic errors arise due to the imperfection of the measurement instruments and measurement setup. They cannot be removed completely, and can be reduced by calibration or mathematically removed after measurements. Random errors are unpredictable errors such as instrument noise error, which arises from various electrical disturbances in the circuits within VNA.

Noise in the measurement system is very probable. It arises due to noise in the environment and within the instruments used in the measurements. Thermal noise caused by the resistive components of the RF components, is one of the most significant noise types in the measurement system [26]. Thermal noise power is given by:

$$P_{\mathrm{N}} = k_{\mathrm{B}} T B \tag{3.9}$$

where $k_{\mathrm{B}} = 1.3807 \times 10^{-23}$ J/K is the Boltzmann's constant, T is the temperature, which is generally assumed to be the room temperature 273 K, and B is the bandwidth. It can be seen from equation (3.9) that noise power is dependent on the temperature and the bandwidth, which means that an increase in bandwidth also increases the noise in the system. In VNA, the bandwidth is limited by the receiver's IF bandwidth, hence noise errors can be reduced. The dynamic range of the measurement system can be increased by increasing the source power which only reduces the low-level noise. Narrowing the IF bandwidth of the receiver, also narrows the bandwidth which is proportional to the noise and applying several sweep averages in the measurement. [18, 26]

3.2. Microwave Material Measurement Techniques

Microwave systems are being used in large number of communication sectors worldwide. Consequently, microwave measurements are necessary to evaluate the behavior of the materials at microwave frequencies. Therefore, several microwave measurement techniques have been developed to test different materials at different environments. The method of measurement depends on the type, shape and size of the MUT. The MUT can be very small or large in dimension, or be in liquid or solid state. Therefore, an appropriate measurement technique has to be selected in order to effectively determine the characteristics of the MUT. Some of the known methods for the characterization of the dielectric properties of the materials are: coaxial probe

method, transmission line (or waveguide) method, resonant cavity method, free-space method, etc. [27]. They are further classified as destructive and non-destructive techniques. In a destructive technique, the sample of the MUT has to be resized and configured to fit inside the measurement instrument before the measurement. In a non-destructive technique, the measurement system does not require reconfiguring the sample, but the material properties can be measured on the location where the MUT exists. This study uses a free-space measurement method for characterization of building materials. Hence, other measurement methods and the difference between these methods are briefly discussed in the next section.

3.2.1. Coaxial Probe Method

Coaxial probe method is one of the widely used methods for the extraction of electromagnetic properties of materials at RF and microwave frequencies. This method uses a coaxial probe to collect the reflection characteristics from the MUT. This method is also known as open-ended coaxial method and it is a non-destructive technique. A coaxial probe is connected to the VNA that collects the reflection and transmission characteristics and displays them as S-parameters. This method is widely used due to its ability to work in wide range of frequencies. The materials are characterized by the reflection measurements achieved by the impedance mismatch between the coaxial probe and the MUT [20]. In this method, the open-end of the coaxial probe is brought in contact with the MUT, and the reflection coefficient is measured. This method is very effective for measuring the properties of liquid and powdered materials. Measurement has to be carried out very precisely when measuring flat surfaces, as a tiny gap at the point of contact between the probe and the MUT can cause catastrophic errors in the measurement data. In case of measurement of liquids, the coaxial probe is dipped into the liquid and the measurements are carried out. A small amount of leakage is expected but the error is considered negligible. Thus, open-ended coaxial probe method is good and accurate for liquid and powdered material and for solid smooth surfaced materials for wide range of frequencies, whereas this method will be ineffectual for rough surface materials due to losses occurring due to the probe with the inequality of the contact between the probe and the surface. Calibration is fairly simple and accurate for this method as only one probe is involved and the cable losses can be compensated quite easily. [27]

3.2.2. Waveguide Method

Transmission line or waveguide method is also widely used, and it has higher accuracy compared to the coaxial method. In this method, sample of the MUT is placed at the center inside the waveguide covering the entire cross-section. The reflection and transmission properties are monitored using a network analyzer to further calculate the characteristics of the MUT. This method is efficient for small material sample as the dimensions of the waveguides are limited. Losses and errors will be significant, if the measurements are not performed precisely. It takes quite a bit of time and accuracy to perform the measurements, as the sample size has to fit accurately enough in the cross-section of the waveguide. Mismatch in dimension may lead to leakage and hence

introduce unexpected results in the measurements. Losses mainly occur due to the waveguide or transmission line materials.

3.2.3. Resonant Cavity Method

Another widely used method is the resonant cavity method. This method relies on the center resonance frequency to extract the electromagnetic properties of the MUT. This method is very accurate for material having low loss-factor and works well in high temperature conditions [27]. This method comprises of a cavity that can be a waveguide of circular or rectangular shape. Firstly, the resonance frequency of the empty cavity is measured, and then the sample is inserted into the tuned cavity and the resonance frequency is measured. Thus, the shift of the center resonance frequency from empty cavity and the filled cavity and even the change in the quality factor, further helps to determine the characteristics of the MUT. It is a destructive technique because the sample has to be resized to be inserted in the cavity. The measurement is done at single frequency or discrete frequency points. The measurement frequency range is very wide for this method varying from 50 MHz to more than 100 GHz [27].

3.2.4. Free-Space Method

Free-space method is a non-destructive, contactless and one of the most widely used approach for material measurements. This method is suitable for the measurement of large objects such as building walls, metal sheets and inhomogeneous materials, and is good for high temperature measurements. The main advantage of this approach over the aforementioned methods is that, there is no need for sample preparation [5]. Free-space measurement systems require antennas, coaxial cables, a network analyzer and the MUT to perform a measurement effectively. Inaccuracies in this method are highly possible due to the phenomenon of free-space transmission and reception. Errors can occur due to several factors such as: diffraction of the edges of the sample, reflections from ground or ceiling, which is not the point of interest or multiple reflections from the surroundings, noise in the environment or in the measurement instrument, losses in cable, depolarization effects of the antennas, large beam footprint of the radiated wave, etc. Therefore, proper calibration of the setup should be carried out to remove errors due to cables and instrument. Advances in the network analyzers have made it very simple to get rid of these error sources. Technique such as time domain gating is used to clear off all the mentioned errors and allows focusing only on the error-free response of the measurements.

Free-space measurement is performed in two ways. The first method is to put the sample in between the two antennas, such that the antennas are focusing each other, i.e. the propagating wave has a normal incident on the MUT. This method is widely used to extract the electromagnetic properties of the materials such as thin film and ceramics, or used as test measurement to calculate the reflection coefficient of a metallic sheet as a reference for further measurements of other materials. This measurement setup requires a sample holder to hold the sample, and an extra set of measurement is required to consider the effect of the sample holder on the total measurement. The second method is the oblique incidence at the MUT. The propagation characteristics of oblique incidence case are discussed in section 2.4.2. Here, the propagating wave from the transmitting

antenna is incident on a MUT and the wave is reflected to the receiver placed at equal distance from the center of the MUT and at equal angle as that of the transmitting antenna. This is done to satisfy Snell's law of reflection ($\theta_i = \theta_r$). A VNA is used to extract the reflection response and display it as S-parameters, which are later converted into the required parameter based on mathematical analysis.

In this study, a free-space measurement system at oblique incidence is utilized to calculate the electromagnetic characteristics of building materials at microwave frequencies. The proposed measurement setup is discussed in detail in the next chapter.

4. MEASUREMENT SCENARIOS AND RESULTS

Microwave measurement utilizing free-space technique was used for the reflection measurements of building materials. All the measurements were performed at the University of Oulu, Finland. Measurements were done at five different places at the university. One test measurement was performed in the anechoic chamber at University of Oulu. Reflection measurements were taken for four different types of walls. The target walls were selected on the basis of smoothness and the materials used for the construction of the walls. This was done in order to find the different behavior of the EM waves to different types of walls. The attenuation and loss of the reflected signals from the building walls depend on the material used for the construction of the wall. Building materials are dielectric in nature, therefore the behavior of the signal with different dielectric materials dictates the efficiency of communication via reflection and transmission from the different dielectric surfaces. Thus, reflection measurements from various dielectric surfaces were collected at different incident angles.

4.1. Measurement Setup

A non-destructive free-space measurement system was proposed for the reflection measurement of building materials. The measurement system consisted of a VNA, four coaxial cables, two wideband dual-polarized Vivaldi antennas. Measurements were taken at different types of walls at several locations at the University of Oulu. The specifications of the devices and the proposed measurement setup are discussed in this section.

Table 1 highlights the input parameters for the setup. These parameters were entered in the VNA manually with the VNA input options.

Table 1: Input Parameters for Reflection Measurements

VNA Output Power	-5 dBm
Number of points	401
Measurement Frequency Range	0.7-7 GHz (6.3 GHz bandwidth)
Antenna height from ground	1.6 m
Intrinsic delay of TX and RX antenna	0.13 m (0.43 ns)
Cable Length	8.0 m

The proposed measurement setup is shown in Figure 9. A 4-port VNA was used as the source to collect the data and display the response in terms of S-parameters. The VNA was a “Keysight PNA-X Network Analyzer N5247A 10MHz-67GHz”. The specifications of VNA are highlighted in detail in [28]. The VNA was operated manually, and the data were collected via a memory-stick and were later analyzed using MATLAB. The wiring of the measurement setup was fairly simple. Four coaxial cables each of length 8 meters were used to connect the VNA to the antennas. Two wideband dual-polarized Vivaldi antennas were used for communication. The advantage of using a dual-polarized antenna was that both polarizations were recorded simultaneously. The crossed-shape form of the antenna enables to achieve orthogonal polarizations. The

dimensions, constructions, radiation pattern and other specification of the antennas are explained in detail in [29]. Some of the specifications of the antenna are listed in Table 2 [29]. As stated in [29], the antennas were good for measurement purposes. Figure 9 shows that port 1 and 3 were used for transmitting and ports 2 and 4 were for receiving. Ports 1 and 2 were connected to the horizontally polarized end of the antennas whereas ports 3 and 4 were connected to the vertically polarized end. Therefore, the S-parameters of interest were S21 for parallel polarization and S43 for perpendicular polarization.

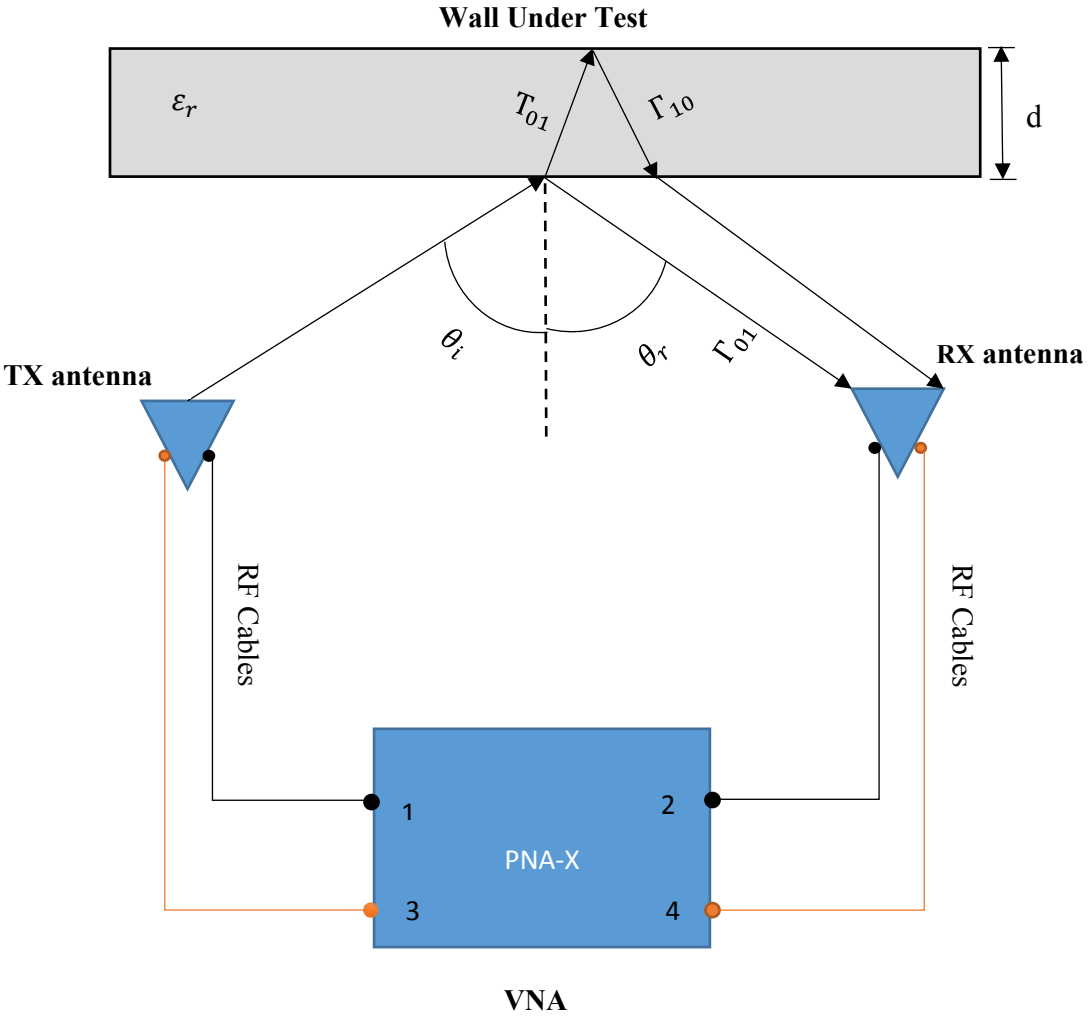

Figure 9: Measurement Setup.

Table 2: Specifications of wideband dual-polarized Vivaldi antenna [29]

-10 dB impedance Bandwidth	0.7-7.30 GHz
Maximum Gain	3.8-11.2 dB
Isolation between antenna ports	>30 dB
Cross-polarization discrimination	>19 dB

4.2. Calibration

Several errors in the measurement arise from the devices being used. The properties of the instruments may change due to the environmental effects. Therefore, proper calibration of the device is required before a measurement to ensure all the effects due to the instruments are removed. The coaxial cables act as the transmission line in measurement systems. Thus, errors in the cables can have significant effects on the measurement data. Many uncertainties and errors in the measurement arise due to bends in the coaxial cables, damage in the coaxial cables and other key factors such as attenuation, impedance mismatch, and phase shift can result due to the cables those depend on time and temperature. Thus, proper calibration standard is needed to nullify the aforementioned errors. Here, the electronic calibration (ECAL) kit for Keysight PNA-X Network Analyzer N5247A was used for calibration. The ECAL kit, mathematically calculates the responses of the cables and compares them to the common standards predefined in the calibration standards to remove the unwanted responses of the cables. The calibration of the cables was further verified by checking the 'through' connection between the cables.

The VNA can also introduce errors due to temperature differences in the components within the VNA. Therefore, it was ensured that the VNA was turn on for sufficient amount of time before the calibration, so that the errors due to the temperature differences of the various components are minimized. There are other noises in the signal from the components of VNA and the environment that cannot be removed. Fortunately, they do not contribute significantly on the responses unless the measurement is carried out in very harsh environments.

4.3. Reference Measurements

Locations for measurements were chosen based on different configuration of walls present in the campus. Four different walls were chosen for the measurements. The walls were considered as infinitely long homogenous slab, as the data for complete construction materials were not available. The types of walls were: outdoor concrete wall, indoor concrete wall, painted indoor brick wall, unpainted indoor porous brick wall with absorber type material. Before the measurements were performed for the walls, a few test measurements were done to check the configuration of devices and responses of the antennas. Line-of-sight measurement was done in order to find the delay between the antennas and as a reference to calculate accurately the reflection coefficient from the metal floor. Each of the measurement scenarios are explained in the following section.

Several reference measurements were taken in the anechoic chamber. These measurements were done as a reference scenario to check the responses of the instruments and the antennas. The test measurements were also used to calculate the reflection coefficient for all the scenarios for which the responses of LOS measurement and reflection from metal surface are necessary.

4.3.1. Line-of-Sight Measurement

Line of sight measurement was performed in the anechoic chamber. HF906 ridge horn antenna was used as the reference antenna (as transmitting antenna) in this case and five dual-polarized wideband Vivaldi antennas were used individually in the receiving end. The responses of the antennas were recorded from 0.7 GHz to 7 GHz, and the S21 parameter was analyzed. The S21 responses of all the antennas were compared to ensure similar radiation properties of the antennas for further measurements. Since different antennas were used for measurement scenarios and test measurements, it was made sure, the antennas responses did not differ significantly from each other. Only horizontal polarization of the antennas was analyzed, therefore the dual-polarized Vivaldi antennas were rotated by 90° to get the responses for both the polarizations of the antenna. Two antennas that were used for the measurement of reflection from a metal floor, show flaws in the responses in one of the polarizations. These flaws were observed due to the broken feed of the antenna and poorly soldered feed of the other antenna. It was observed that the antennas were functioning properly during the previous metal floor reflection measurements, and the soldering was done on a later date. Therefore, the data taken for other cases did not have any errors due to damaged antennas. The antennas used for this case are shown in Figure 10 and 11, the measurement setup for LOS test case is shown in Figure 12 and S21 responses of all the antennas are shown in Figure 13 and 14 for horizontal and vertical polarization, respectively.

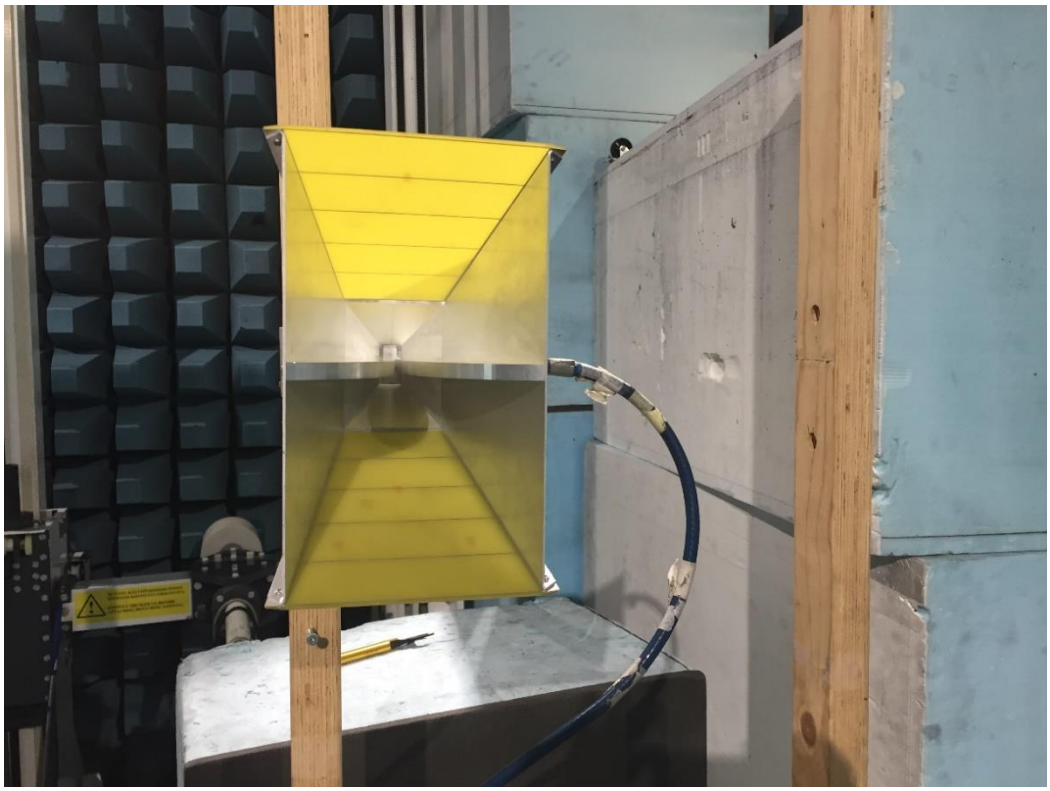

Figure 10. HF906 ridge antenna

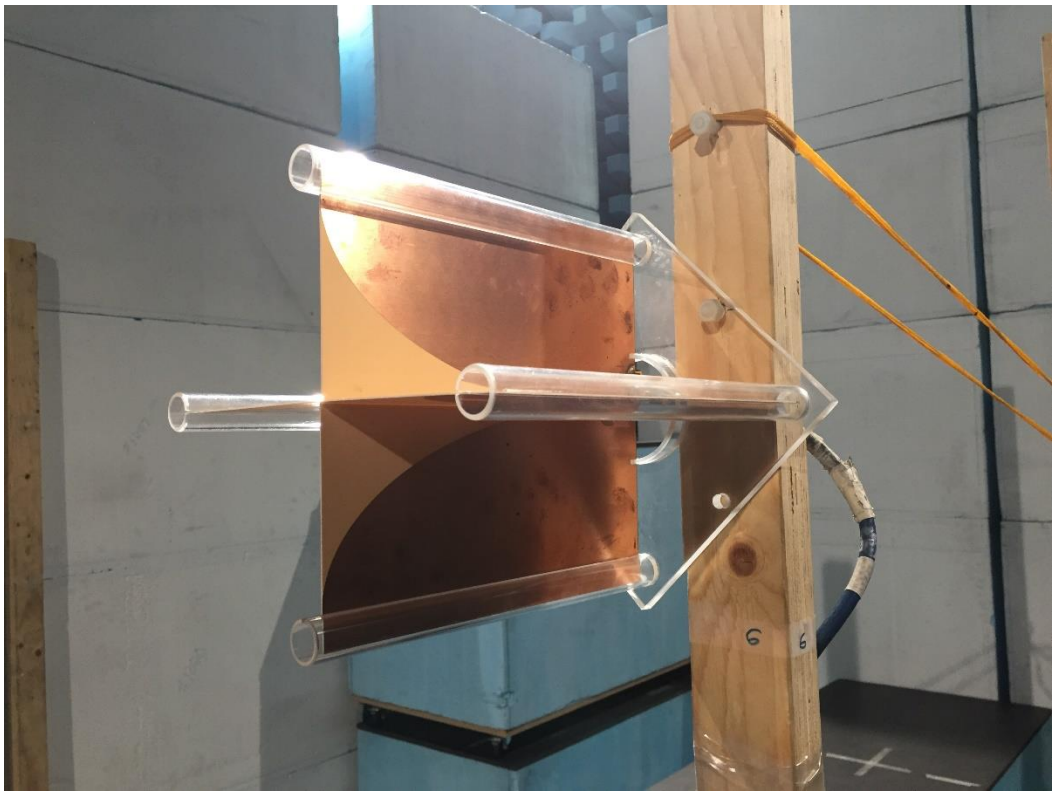

Figure 11. Dual polarized wideband Vivaldi antenna

The absorbers as seen in Figure 12, attenuate the ground reflected signals that may have significant effects on the total received signal. The antennas were kept at the same height at approximately 1.6 m to ensure maximum power transmission. The antennas were separated by a distance of 4.5 m. The electrical delay introduced by the antennas that were added into the network after calibration was approximated to be 0.43 ns ≙ 0.13 m. Therefore, this delay is taken into account, and the total distance between the antennas is taken as 4.68 m for better accuracy.

The frequency response plots for both polarizations of the antennas are shown in Figures 13 and 14. In Figure 13, there is no response for antenna 1 due to the broken feed of the antenna for horizontal polarized face. Free-space loss was calculated and plotted in Figure 13 from 1.5 GHz to 6.5 GHz at 1 GHz difference using Friis transmission equation. Gain of both antennas varied from 8 dB at lower frequencies to 11 dB at higher frequencies. Thus, the theoretical free-space loss is in good agreement with the measured values. It can be seen in Figure 14 that antenna 8 has poorest response. The behavior of this antenna was observed to be a result of improper soldering, carried out by another user after the measurement of the metal floor reflection. Time domain gating was applied with a gate span of 0.5 ns to remove all unwanted multiple reflections and to focus only on the LOS signal.

Figure 12. Line-of-Sight Measurement setup.

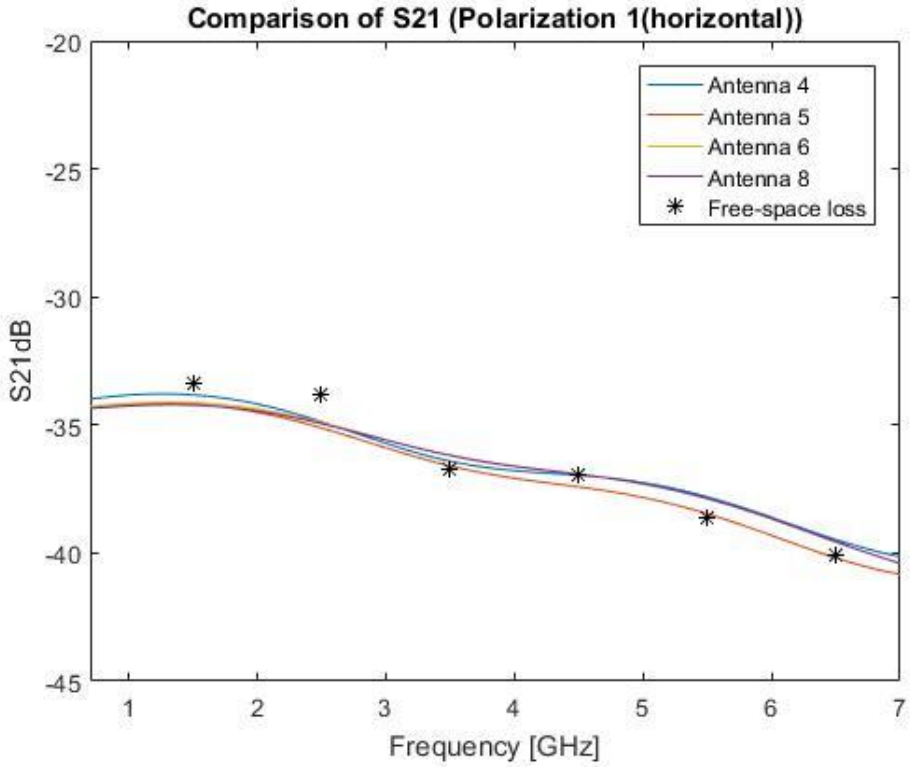

Figure 13: Antenna response comparison (horizontal polarization)

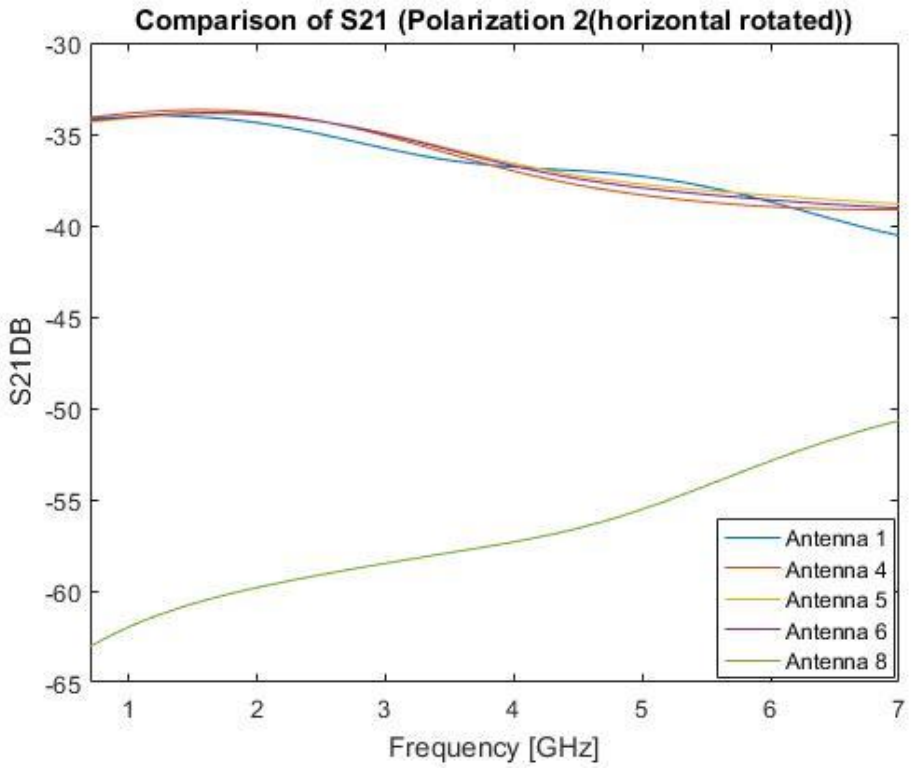

Figure 14: Antenna response comparison (vertical polarization)

4.3.2. Metal Floor Oblique Incidence Measurement

Reflection measurement was performed in the anechoic chamber. This measurement was necessary to calculate the reflection coefficient for other scenarios; this will be explained in other section. The reflection coefficient from the metal floor is close to 1 as all the signal is expected to get reflected from the surface of the metal floor. The measurement was done with two Vivaldi antennas focused at the chamber's metal floor. The separation between the antennas was 3.22 m. The height of the antenna from the ground was 1.26 m. Thus, they were focused at an incidence angle of approximately 52°. The measurement setup is shown in Figure 15. Both polarizations were measured simultaneously by the VNA. The absolute value of reflection coefficient for this measurement was calculated by normalizing the receive electric field strength from the reflection of the metal floor with the received field strength for LOS measurement. The following equation (4.1), defines the calculation of reflection coefficient in this case [30].

$$|\Gamma| = \frac{d_1 + d_2}{d_{\mathrm{LOS}}}\left(\frac{S21_{\mathrm{refl}}}{S21_{\mathrm{LOS}}}\right) \tag{4.1}$$

Here, d_1 and d_2 represent the total path length from transmitter to the receiver via reflection from the metal floor and d_{LOS} represents the LOS path length. This term is necessary to scale the measurements to account for the path loss difference in the two measurements. The absolute value of reflection coefficient for the metal floor was found to be approximately 0.9 for both polarizations, which is close to 1 and can be reliably

used for all the other scenarios as the reference case. Time domain gating was used to separate the LOS signal and other multiple reflections from the reflected signal from the metal floor.

Figure 15. Metal floor Reflection Measurement Setup

4.4. Reflection Measurement of Building Materials

Oblique reflection measurements were taken at various places in the University of Oulu. Different types of walls were considered as the MUT. They were categorized based on the construction materials used and these materials are considered dielectric in nature. Different dielectric materials have different permittivity values. Thus, complex relative permittivity for these materials was estimated using the reflected field at different incident angles. Measurements were taken for two angles in the outdoor scenario, three angles for indoor scenarios and four angles for the last scenario. With limited working hours, repeated configuration of the measurement equipment and traffic at the University, measurement at several incident angles was very difficult to achieve. The antennas were kept at sufficient distances from the walls to achieve the far field criteria for electromagnetic radiation. All four scenarios and measurement setups are described in detail in the following section. After completing all scenarios, a reference case of a concrete wall was measured positioning the antennas symmetrically about the normal at 12 spots from 10° up to 75° along a half circle

4.4.1. Outdoor Measurement

The location of wall was outside the door E3 at the University of Oulu. Two Vivaldi antennas were mounted on two wooden structures and the connections with the VNA were made using 8 m coaxial cables. The measurement setup for outdoor scenario is shown in Figure 16. The measured wall was in the shadowed region of the building i.e. it did not get any sunlight, therefore the structure was damped and contained moisture. The thickness of the measured wall was 0.497 m.

Figure 16. Outdoor Measurement Setup

Outdoor 1: The distance between the antennas was fixed at 3.8 m. The measured wall was at the distance of 2.75 m from the antennas. Distances were measured carefully to ensure the angle of incidence and angle of reflection to be equal to each other. The angle of incidence was 34.6° (0.605 radians). The path length of the reflected wave from surface was calculated to be 6.685 m. The maximum received signal strength from the surface of the wall was -49.58 dB and -46.82 dB for parallel and perpendicular polarization, respectively. Gating was applied using the VNA, with the gate span of 2 ns and multiple reflections from the surroundings and LOS signal were removed from the gated response.

Outdoor 2: The transmit and receive antennas were placed 1.9 m from the wall. The total reflected path-length was measured to be 6.2 m. The distance between the antennas was 4.9 m. The angle of incidence in this scenario was 52.2° (0.911 radians). The maximum received signal strength was -52.15 dB and -45.04 dB for parallel and perpendicular polarization, respectively.

From both measurement points, it can be seen that the total reflected path and the distance of the antennas from the wall were reduced whereas the LOS distance is greater in case of *Outdoor 2*. The effect of change in distance and angle can be observed and verified easily from the Delay domain data, shown in Figure 17 and 18. It is observed that perpendicularly polarized wave reflects more compared to parallelly polarized, and parallel polarization has more tendency to penetrate inside the material as compared to perpendicular polarization. A few peaks with lower strength and slightly longer delay than the main reflected wave can be observed from the figures. One of the peaks with smallest delay is assumed to be the first internally reflected wave from within the concrete.

Measurements at only two points were taken for this scenario, which is expected to be enough to estimate the permittivity profile for the outdoor wall as a function of incident angle. The research suggests that more points allow better estimation of the dielectric properties of material for this approach. The calculation for the dielectric constant and the result for this scenario will be presented later in the chapter.

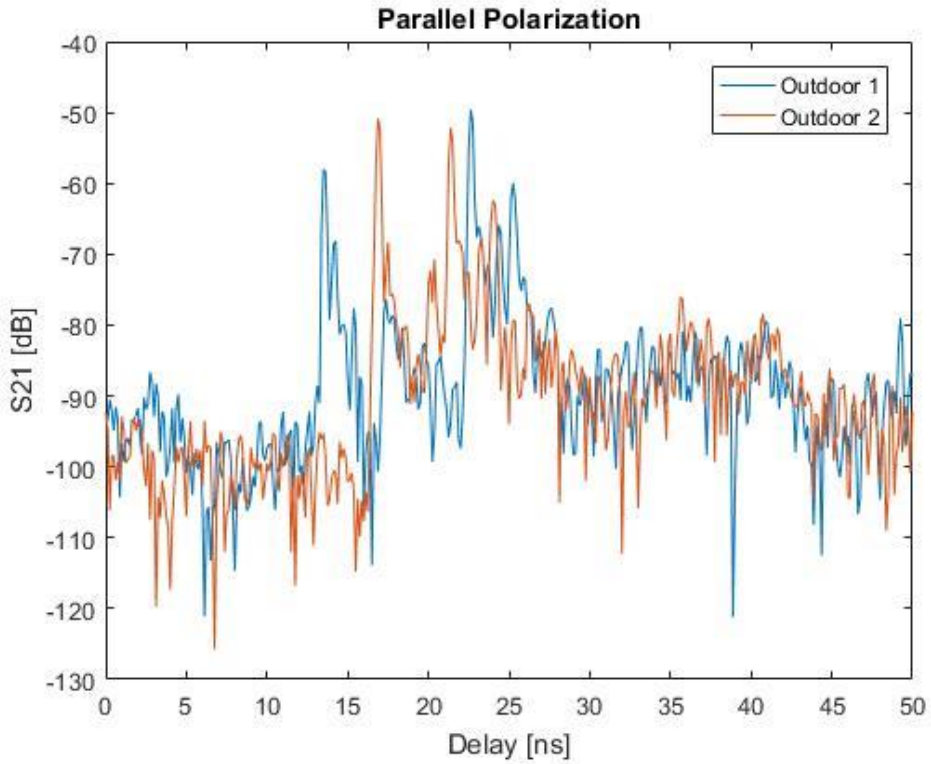

Figure 17. Delay Response Comparison (Parallel Polarization)

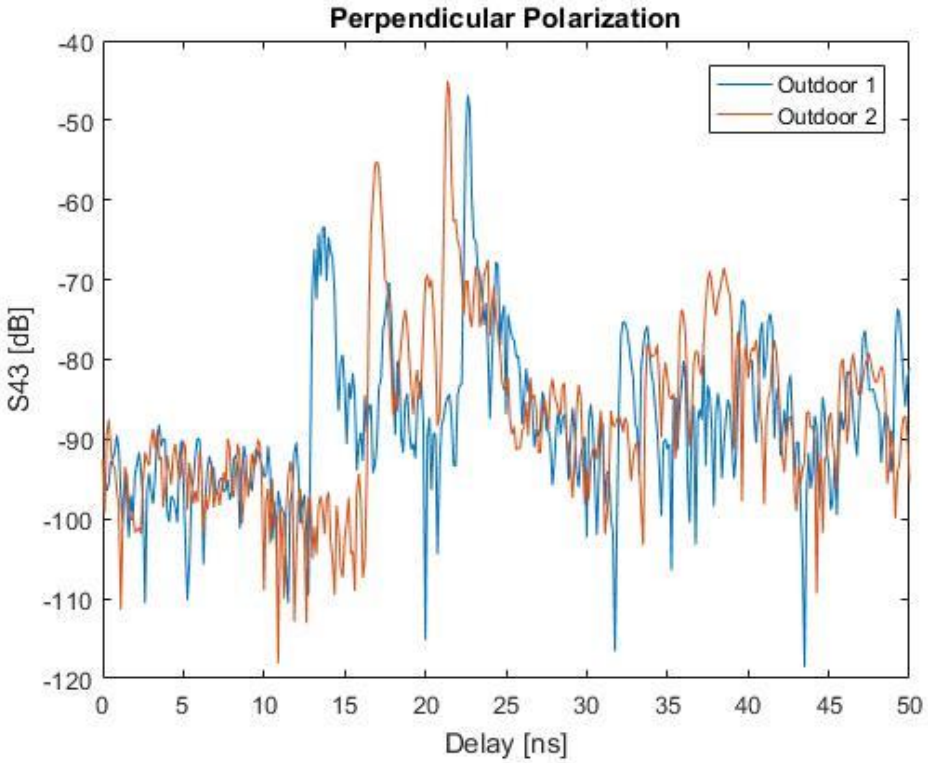

Figure 18: Delay Response Comparison (Perpendicular Polarization)

4.4.2. Indoor Concrete Wall

Indoor measurement was performed inside the University of Oulu. The wall was chosen on a corridor (close to Kastari restaurant). It was a painted, smooth and dry concrete wall. Therefore, no surface scattering was expected. Measurements were performed twice at the same wall, once with three different randomly chosen incident angles, followed by twelve symmetrically spaced incident angles. A boundary fence was formed around the setup area to ensure the traffic at the University did not interfere with the experiment. The thickness of the wall was measured to be 0.13 m. The measurement setup is shown in Figure 19.

Indoor Concrete 1: The antennas were placed 2.74 m from the wall. The antennas were kept 5.84 m apart. The total reflected path of 7.9 m and the incident angle of 48° (0.8378 radians) were calculated using the measured distances. Time domain response showed there were no significant reflections from the ceiling or ground that would interfere with the interested reflected wave. However, gating was applied with a gate span of 1 ns to eliminate the effects due to LOS signal and other multiple reflections. The received signal strength from the surface reflection was -58.46 dB for parallel polarization and -49.8 dB for perpendicular polarized wave.

Indoor Concrete 2: The distance between the antennas and the wall was varied to achieve measurement at a different angle of incidence. The distance between the antennas was 5.8m and the distance from the antenna to the wall was 1.97 m. The calculated total reflected path was 7.03 m. The angle of incidence was 56° (0.9774

radians). The received reflected signal strength was -64.15 dB and -47.3 dB for parallel and perpendicular polarization, respectively.

Figure 19. Indoor Concrete Wall Setup

Indoor Concrete 3: The distance between the antennas was kept the same as in the previous case, i.e. 5.8 m. The distance from the antenna to the wall was 1.8 m. The calculated angle only varied by approximately 2°, i.e. measured incident angle in this case was 58.26° (1.0168 radians). The total reflected path length was 6.84 m, which is close to the previous case. The maximum received signal strength for parallel polarization was -61.11 dB and -46.9 dB for perpendicular polarization.

Measured responses are plotted in delay domain and compared in Figures 20 and 21 for parallel and perpendicular polarization, respectively. Perpendicularly polarized wave reflected much better than parallelly polarized wave. It can be seen that the received signal strength for perpendicular polarization is increasing as the angle of incidence is increased. The low value of signal strength in case of parallel polarization compared to perpendicular polarization can be due to the angle of incidence being close to the Brewster angle. At Brewster angle, the parallelly polarized wave completely transmits through the medium i.e. there will be no reflection. It can be observed from Figures 20 and 21 that the delay difference between the peaks of all three measurements gives good understanding of the effects of changing the angle of incidence on the delay response of the received signal.

Here, the gated responses for both polarizations are shown. The delay data without the gate had many multiple reflections, which prevented the responses to be viewed clearly for all the measurements in a single plot. Therefore, only the gated delay response is shown here.

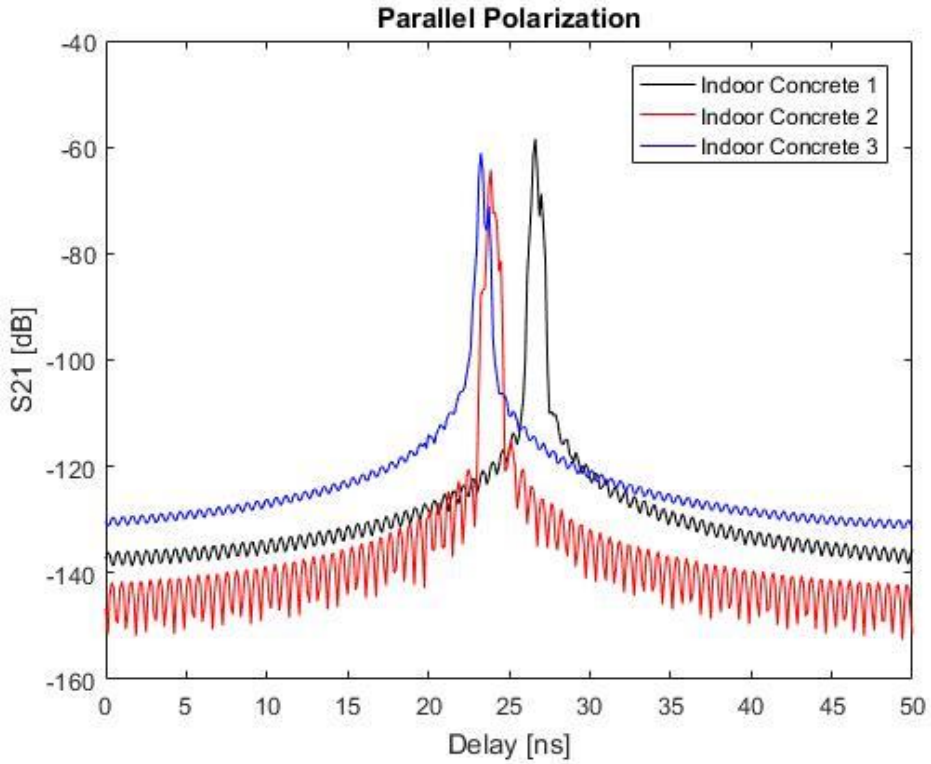

Figure 20. Gated Response (Parallel Polarization)

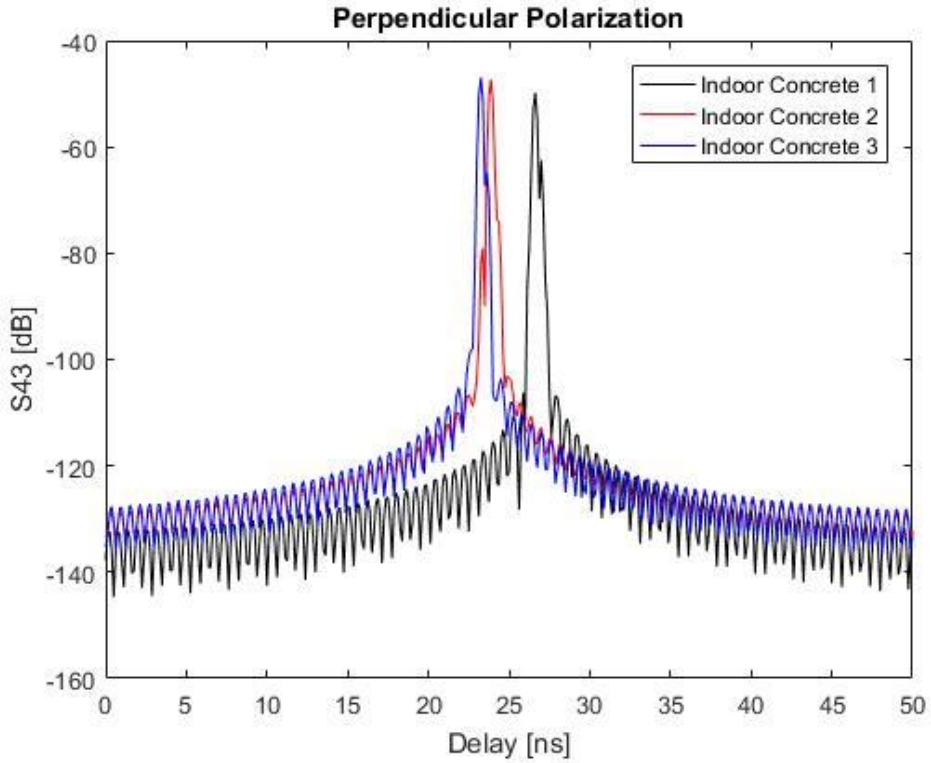

Figure 21. Gated Response (Perpendicular Polarization)

Indoor Concrete Multiple Angles: Measurements were performed at seven equally spaced incident angles from 10° to 70° with a difference of 10° between the consecutive angles. The incident angles after 50° were close to the Brewster angle, therefore, the angles were further equally divided with a difference of 2.5° from 55° to 65°. The last angle of incidence was 75°. Therefore, total of twelve incident angles were investigated during this measurement. A semicircle was formed to ensure the distance of the antennas from the point of interest in the wall remained the same for all incident angles. The distance from the center of the wall to the antennas was 2.61m. The measurement setup is shown in Figure 22. The received signal showed good agreement for both polarizations. The signal strength decreased steadily until the angle reached near Brewster angle and started increasing for higher incident angles, which satisfied the behavior of electromagnetic waves at parallel polarization. Steady increase was witnessed in the received signal level for perpendicular polarization for all angles of incidence. Blocks of absorbers were used to eliminate ceiling and floor reflection and LOS signal. Time gating was applied with a gate span of 0.3 ns for all the incident angles. Thus, all other multiple reflections from the environment were removed.

Figure 22. Multiple Angle Setup

4.4.3. Indoor Classroom Brick Wall Measurement

Reflection measurement was performed in a classroom wall made of bricks. The bricks used for the construction of the wall were porous in nature i.e. they had several holes which made the wall surface very rough in nature. The bricks were placed in front of a foam type material, which generally acts as an absorbing material for electromagnetic waves. The distance of the foam from the outer surface of the wall was approximately 0.114 m. The thickness of the wall was approximately 0.268 m. Measurements were taken at four different angles varying the distance between the antennas and the distance to the wall. The measurement setup is shown in Figure 23. The four different measurement setups are explained below.

Figure 23. Classroom Measurement Setup

Brick Wall 1: The antennas were separated by a distance of 4.46 m. The distance of the antennas from the brick wall was 2.67 m. The angle of incidence and the total reflected signal path in this case was calculated as 40° (0.6981 radians) and 6.96 m, respectively. The maximum reflected signal strength for parallel polarization was -66.45 dB and -75.01 dB for perpendicular polarization. Gating was applied with a span of 1.0 ns to get the clear response from the reflecting surface eliminating all other multiple reflections.

Brick Wall 2: The incident angle was decreased in this scenario by decreasing the distance between the antennas to 3.7 m but the distance of the wall from the antennas were kept approximately same i.e. 2.7 m. The angle of incidence decreased nearly by slightly more than 5°, i.e., 34.41° (0.6006 radians). The maximum received signal strength from reflection was -72.96 dB for parallel and -75.58 dB for perpendicular polarization. The reflected peaks were very hard to separate out therefore, gating was applied with a narrower gate span of 0.5 ns to get better delay resolution.

Brick Wall 3: The angle of incidence is further decreased in this scenario to 12.44° (0.2171) which is 22° less than the previous case. The total reflected path was 5.53 m. The distance from the antenna to the wall was kept the same, i.e. 2.7 m, whereas the antenna separation was reduced to 1.2 m. The received power strength measured for parallel polarization was -85.15 dB and for perpendicular polarization was -84.31 dB. It can be observed from the received signal value that when the angle of incidence is reduced, both the polarizations give close response. Thus, at normal incidence both the polarization behaves similarly.

Brick Wall 4: This setup was the final measurement scenario for classroom case. The angle of incidence was increased for this case to 54° (0.9425 radians) by increasing the distance between the antennas to 1.66 m and reducing its distance to the wall to 1.17 m. The total reflected path in this case was 4.06 m. Two different significant peaks were observed that were coming from the reflected surface. It could be the structure and the roughness of the bricks that gave such unusual reflections. The maximum reflected signal strength for parallel was -58.84 dB and -57.42 dB for perpendicular polarization.

The behavior of electromagnetic propagation was recorded for the brick wall mentioned above. The measurement at four different angles gave very different result. The non-gated version of the total received signal in delay domain is plotted in Figure 24 and 25 for both polarizations respectively.

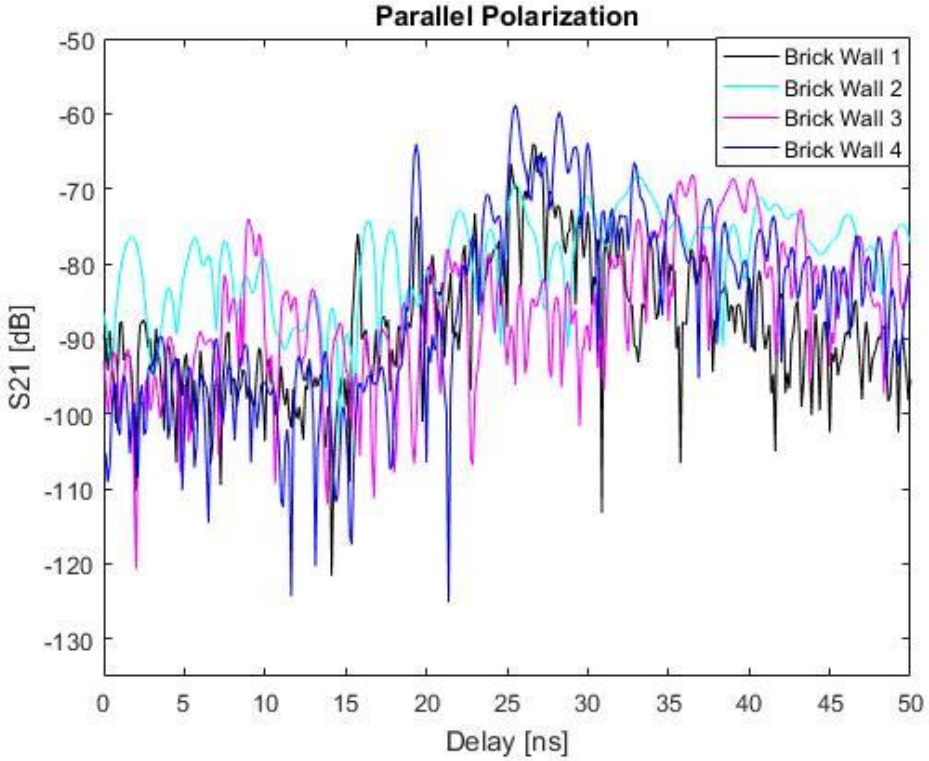

Figure 24. Delay Response (Parallel Polarization)

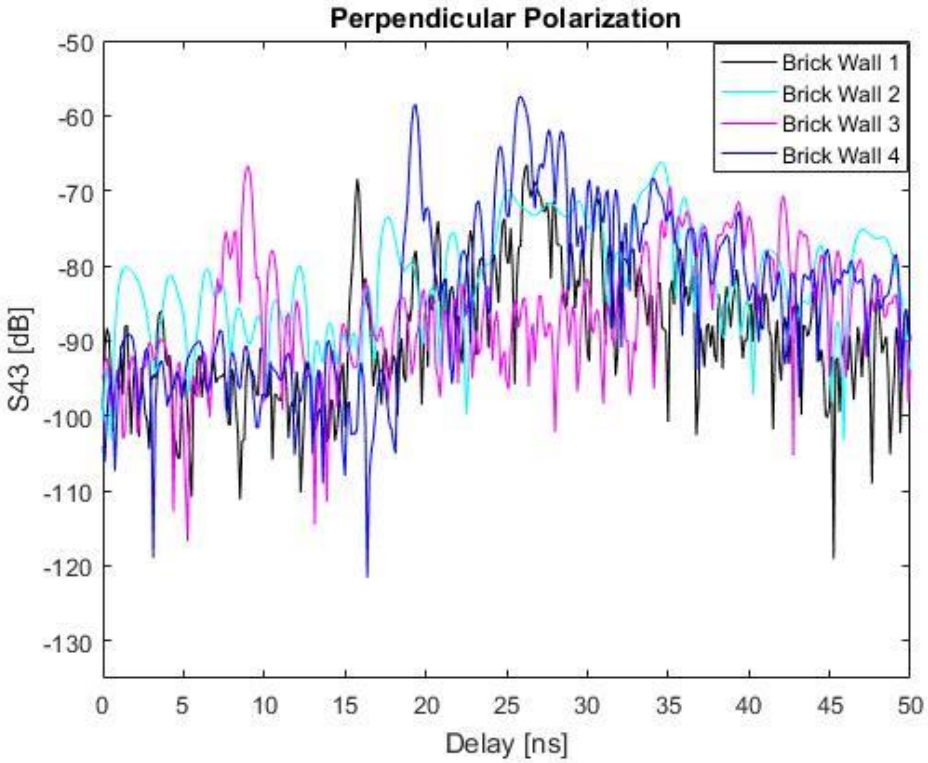

Figure 25. Delay Response (Perpendicular Polarization)

It can be observed from the delay response plots that; the received signal strength is increasing with respect to increase in the incident angle. *Brick Wall 4* gives the best response in comparison to other measurements. The holes in the bricks and the foam behind them are absorbing the signal more when the angle of incidence is smaller. In *Brick Wall 3*, for which the incident angle was 12.44°, we receive very low signal, in the order of -80 dB and below for both polarizations. Thus, the pores in the bricks and the foam attenuate the signal significantly at low incident angles. As the angle of incidence is increased, the electromagnetic waves tend to reflect more from the surface in this case. The behavior of signal in terms of frequency response can be analyzed easily from Figure 26 and 27. These frequency domain plot represents the frequency content in the reflected signal. This plot was achieved by applying gating in delay domain to capture the reflected peak and converting the signal to frequency domain using Fourier transform.

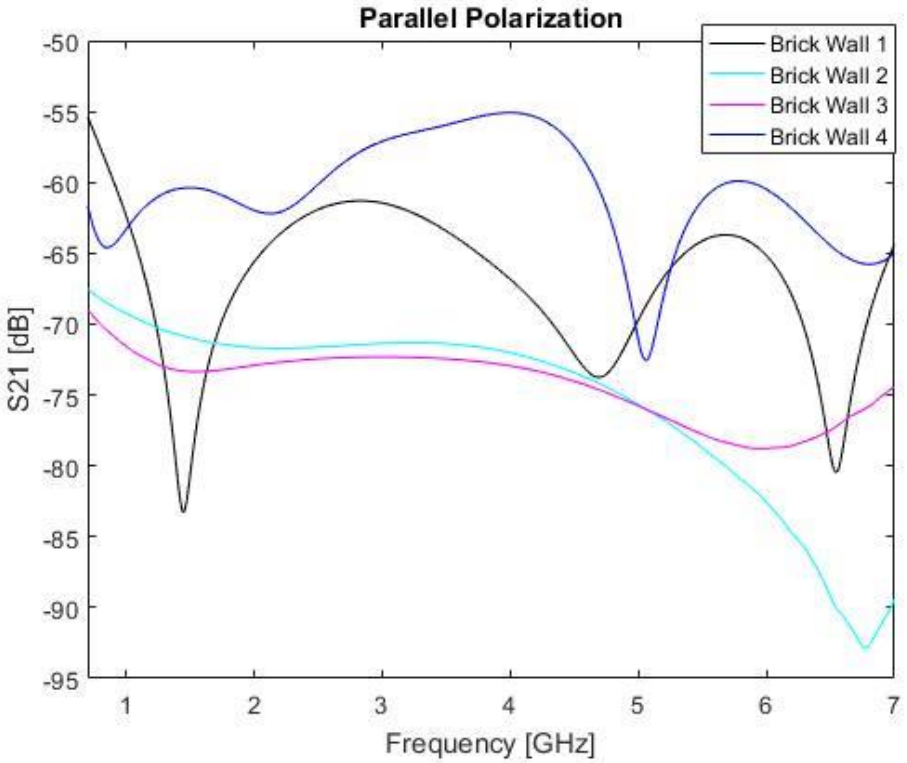

Figure 26. Gated Frequency Response (Parallel)

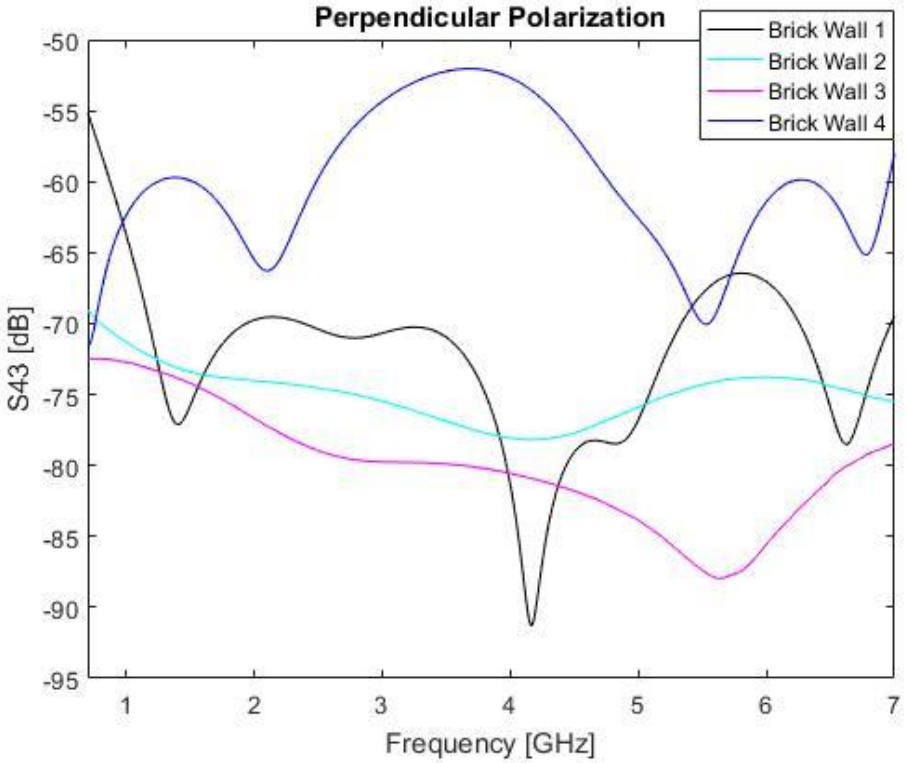

Figure 27. Gated Frequency Response (Perpendicular)

It can be observed in the figure above, *Brick Wall 1* and *Brick Wall 4* show variation over the entire frequency range whereas *Brick Wall 2* and *Brick Wall 3* have smooth responses. It is due to the gate span applied in the delay response data that determines the smoothness in the frequency response. The gate span of 0.5 ns was applied for *Brick*

Wall 2 and *Brick Wall 3* whereas 1 ns gate span was applied in case of *Brick Wall 1* and *Brick Wall 4*.

4.4.4. Painted Brick Wall Measurement

The measurements in this scenario were taken in the Tellus Library at the University of Oulu. The wall to be measured was made from brick wall, supported by concrete. The wall was painted. Measurements were taken at three different angles by varying the distance between the antennas and the wall. The area around the measurement setup was guarded by a boundary so that the traffic in the library did not disturb the experimental setup. The height of the ceiling was 3.45 m from the ground. The thickness of the wall was measured to be 0.2 m The measurement setup is shown in Figure 28. The three measurement setups for this measurement are explained below.

Painted Brick 1: The antennas were separated by 3.9 m. The distance of the antennas from the wall was fixed at 2.48 m. The angle of incidence was 38.18° (0.67 radians). The total reflected path was calculated and verified from the delay response data to be 6.3 m (21 ns delay). The maximum reflected signal strength for both polarizations were -52.61 dB and -48.1 dB. In this system, perpendicular polarization has better reflection response as compared to parallel.

Figure 28. Painted Brick Wall Measurement Setup.

Painted Brick 2: The incident angle was increased by increasing the distance between the antennas to 4.8m. The antennas were taken closer to the walls i.e. 0.86 m. The angle was almost doubled in this case, and it was measured to be 70.28° (1.2267 radians). The

total reflected path was 5.08 m (19.3 ns). The LOS distance and the total reflected path are close to each other, therefore we witnessed small delay difference between the two signal peaks. The maximum received signal strength for both polarizations were -55.59 dB and -41.32 dB for both polarizations. The low value for parallel polarization can be explained by the tendency of this polarization to transmit through the medium, which is less in case of perpendicular polarization.

Painted Brick 3: The separation between the antennas was further increased in this case to 6.68 m. The distance of the antennas to the wall is fixed at 0.95 m. The angle of incidence in this scenario was 74.27° (1.2962 radians). The maximum reflected signal strength of -51.17 dB and -51.27 dB was recorded for parallel and perpendicular polarization respectively. At this angle, both polarizations are behaving in similar manner.

The measurement data of all three scenarios of the brick wall were investigated. A delayed reflected peak higher than that of the interested peak was noticed in the delay response for all measurements. It is suspected that this unknown peak might be coming from reflection through some metal structure inside the wall or from other metal structures present in the surroundings or the ceiling. However, gating was applied to separate out unknown reflections, as well as LOS signal. The ceiling height was measured and the reflected path from the ceiling was analyzed later, which gave a clear intuition that the strong reflection might be the result of reflection from the ceiling. Another suspected cause of the unusual reflected signal can be the result of reflection from a metal structure present in inside the wall. The measured angles for measurement 2 and 3 in this case are above 60°, which can lead to significant measurement error due to direct line-of sight components at large angles [6].

The reflected signal can be analyzed in the delay domain plots shown below in Figure 29 and 30. It can be observed in the delay domain plots that for both polarizations, measurements at all angle show an unknown peak next to the interested reflected peak. From geometry and ray tracing, the unknown peaks give good approximation that they are reflected waves from the ceiling. However, both of the polarization give good reflection behavior in case of painted brick wall for all measured incident angles.

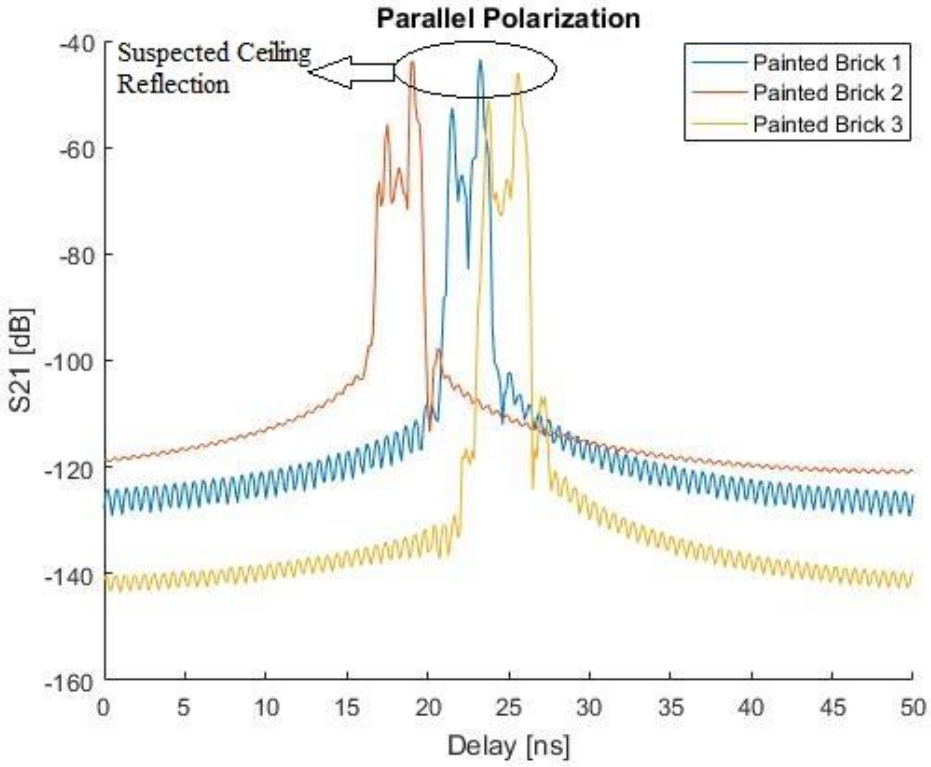

Figure 29. Gated Delay Response (Parallel)

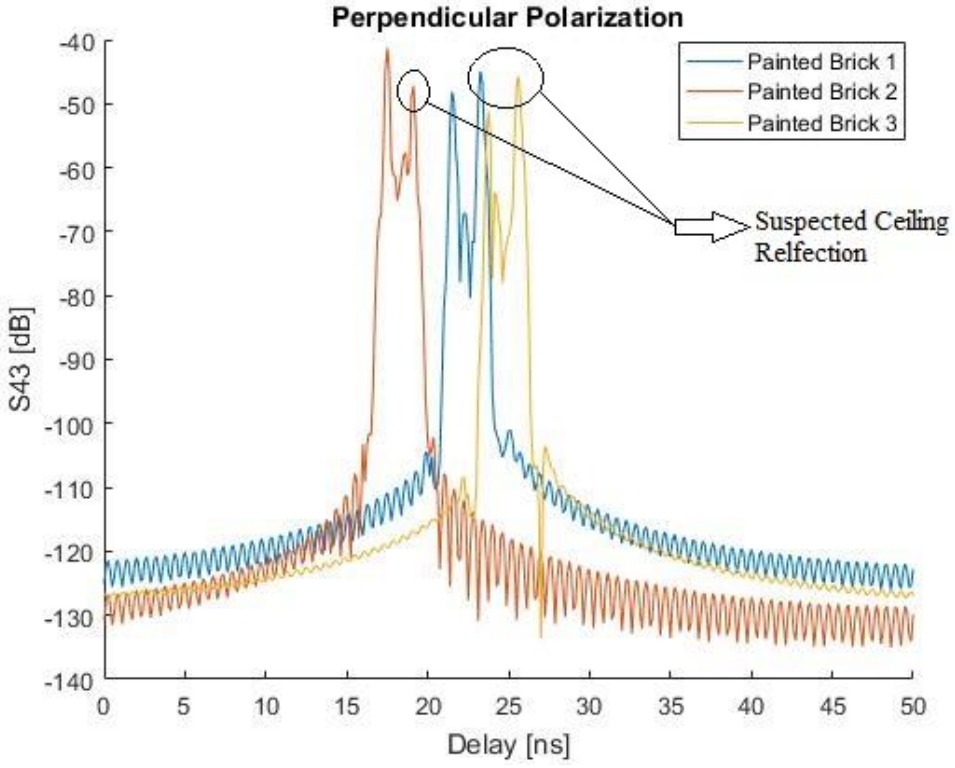

Figure 30. Gated Delay Response (Perpendicular)

4.5. Estimation of Dielectric Constant

Dielectric properties of the building walls are the key parameters for designing an indoor and outdoor propagation models. The propagation of electromagnetic waves depends on the reflection and transmission characteristics from different material in the surrounding. Therefore, the knowledge of the dielectric constant and loss tangent enables to design efficient propagation system [6]. In this study, the dielectric constant (relative permittivity) of different walls is estimated as a function of incidence angle and frequency. A free-space measurement system for oblique reflection at various angle of incidence is investigated for four different type of walls. No straightforward equation to calculate the permittivity profile of a material using oblique incident reflected waves is found in the investigated literature. Thus, estimation of dielectric constant is an optimization problem, where a suitable objective function is minimized to obtain the estimated value for dielectric constant [1]. The estimated value will be compared to other literatures, so that the dielectric constant will match the existing values for measurements presented in various studies [1,6-9].

In previous publications [1,6-9], reflection from several incident angles were investigated for all the cases at a single frequency or few discrete frequency points. However, in this study, measurement at only few angle of incidence was done due to time constraint and complexity and traffic in the measurement environment over the frequency range 0.7-7 GHz The equations, algorithm and objective function for the estimation of dielectric constant are discussed in the next section.

Estimation of dielectric constant is done as an optimization process by minimizing appropriate objective function. The objective function takes the mean of difference between the theoretical and the measured value of reflection coefficient over a range of frequency considering the complex relative permittivity constant, which yields a good estimation of dielectric properties of the MUT. A non-linear least squares method is used to fit the theoretical value to the measured value of reflection coefficient, which gives the estimate of dielectric constant. MATLAB is used as a tool for all calculations in this study. A MATLAB function, *lsqnonlin* is used for optimization purpose [31].The algorithm requires a good initial value of ε_r to converge to a better result. However, it is very sensitive to the initial value. The algorithm searches for the local minimum based on the initial values and when there are multiple local minima, the algorithm converges to the local minimum that gives the smallest function value, which is the global minimum. However, initial values were chosen based on the results from other scientific publications and the extracted results were in the range of the values used as references. Here, the absolute value of reflection coefficient from the measurement is obtained by normalizing the reflected signal from the wall by that of the metal floor, for which the absolute value of reflection coefficient is close to unity.

The theoretical value of reflection coefficient was investigated utilizing different scientific publications mentioned in the references. A theoretical model with infinite reflections is applied. The theoretical reflection coefficient is given by equation (2.20) and equation (2.21). This equation shows that reflection coefficient is a function of thickness of the material, frequency (λ = c/f), relative permittivity, incident angle and wave polarization. The Fresnel coefficients are given in the previous chapters by (2.22) and (2.23) for parallel and perpendicular polarization, respectively. Equation (4.2) is used to calculate the measured reflection coefficient, and is given by:

$$|\Gamma_{meas}| = \frac{d_{\text{refl}}}{d_{\text{m\_refl}}}\left(\frac{\text{S21}_{\text{refl}}}{\text{S21}_{\text{m\_refl}}}\right) \tag{4.2}$$

Here, d_{refl} is the total reflected path from the wall and $d_{\text{m\_refl}}$ is the reflected distance from the metal floor. These distances are required to scale the two measured values. $S21_{\text{refl}}$ and $S21_{\text{m\_refl}}$ are the received reflected signal strength for measured wall and the metal floor, respectively.

The error function presented in equation (4.3) is the suitable objective function in this study. MATLAB function *lsqnonlin,* is used to fit the measured value to the theoretical value by finding the minimum error between two values determined by the estimate of ε_r. The real and imaginary parts of the permittivity are kept constant over the range of frequency. This algorithm requires an initial guess of ε_r to start the calculation. After a few iterations, as the value of ε_r gives minimum difference between the theoretical and measured value, the iteration stops and gives the estimated value of ε_r. A flow chart for the process of estimation of relative permittivity is shown in the Appendix.

The objective function is defined as

$$\text{F}(\varepsilon_r) = \frac{1}{N_\theta . N_f}\sum_{i=1}^{N_\theta}\sum_{k=1}^{N_f}\left|\Gamma_{\text{tot}_{\text{thy}}}(\theta_i, f_k, \varepsilon_r', \varepsilon_r'') - \Gamma_{meas}(\theta_i, f_k)\right| \tag{4.3}$$

Where, N_θ and N_f represent the number of incident angle and number of frequency samples, respectively. θ_i represents the i^{th} incident angle, f_k is the k^{th} frequency sample. $\Gamma_{\text{tot}_{\text{thy}}}$ and Γ_{meas} represent theoretical reflection coefficient and measured reflection coefficient, respectively. $\varepsilon_r', \varepsilon_r''$ are the dielectric constant and loss factor of the MUT and are considered constant over the chosen frequency band.

4.6. Results

Calculation of accurate value of dielectric constant is not possible; therefore, the estimation of electromagnetic properties of building walls was done by investigating the reflected fields as the function of angle of incidence over a 0.7-7 GHz frequency range. However, frequencies at the lower and upper end of the band were omitted due to possibility of error. Therefore, a suitable band within the mentioned range of frequency, where the antennas has best response was chosen for better results. The theoretical reflection coefficient was calculated by fitting it to the measured value of reflection coefficient for suitable value of dielectric constant. The real part of ε_r gives the dielectric constant that denotes the amount of energy stored in the material and the imaginary part gives the loss of electromagnetic energy in form of heat. With this information loss tangent can be calculate using equation (2.15). The higher value of real part of ε_r denotes high reflection characteristics of material and lower value of imaginary part of ε_r indicates low loss in the medium and higher transmission through the medium. The results for all the scenarios are presented with the comparison with previous findings from the literature in this section.

4.6.1. Outdoor Wall

Complex relative permittivity was calculated using only two measured incident angles in this scenario. The concrete wall measured was moist and damp in nature. The thickness of the wall was 0.497 m. The gated received signal from the interested reflection point on the concrete wall was selected and normalized with the received signal from the metal floor measurement to get the absolute value of measured total reflection coefficient. The measured total reflection coefficients in this case were calculated from 0.7-7 GHz at different discrete frequency points for incident angles 34.6° and 52.2°, respectively. The frequencies were chosen where the theoretical reflection coefficient values gave meaningful response according to the estimated ε_r. A good initial value of ε_r is required for *lsqnonlin* algorithm to converge to a good estimate of ε_r. The algorithm is sensitive to the initial value. However, it converges within the range of values comparable to the values in the literature [8]. The estimated value of dielectric constant for parallel polarization varied between 4.2 – 6.5 and for perpendicular polarization between 3.7 – 7.3 for various frequencies. The comparison between the theoretical and measured reflection coefficient and the value of complex permittivity at various frequencies are given in Figure 31 and 32. The ε_r value was also estimated for frequency range from 3-6.5 GHz considering $\varepsilon_r$constant over the frequency range. The estimated value of ε_r in this approach was 5.1437-1.0549i and 5.7663-0.9310i for parallel and perpendicular polarization, respectively. Loss tangent for parallel polarization was calculated to be 0.2051 and 0.1615 for perpendicular polarization. The relation between reflection coefficient for the estimated ε_r at various frequency is observed. The standard value of dielectric constant of concrete varies with the moisture content in the concrete (i.e., from 3~15) [3]. The unrealistic variation of the permittivity is due to the nature of the concrete wall. Since, the wall was in moist condition and did not receive sunlight throughout the year. Therefore, the moisture content in the concrete is expected to influence the relative permittivity. High loss factor value in this case could be the result of the wall thickness, moisture, heterogeneity of the concrete wall. The concrete wall is supported by iron grid from within and may contain other layers, which explains the high value of loss factor. Therefore, this scenario gives a good estimate of permittivity. However, measurements at several incident angles can better determine the complete reflection behavior and good estimate of dielectric constant. Estimation of dielectric properties can be done by measurement at a single point but the uncertainty of errors in this case will be large. Thus, measurements at several angles decreases the error in the estimated value of ε_r.

The Brewster angle at a single frequency is shown in Figure 33 and was found to be 65.02° at 6 GHz. However, Brewster's angle is a function of ε_r, as can be observed in Figure 31. The lowest value of reflection coefficient for parallel polarization is not zero if the medium is lossy. Thus, in conclusion complete transmission of radio waves in a lossy medium is not probable.

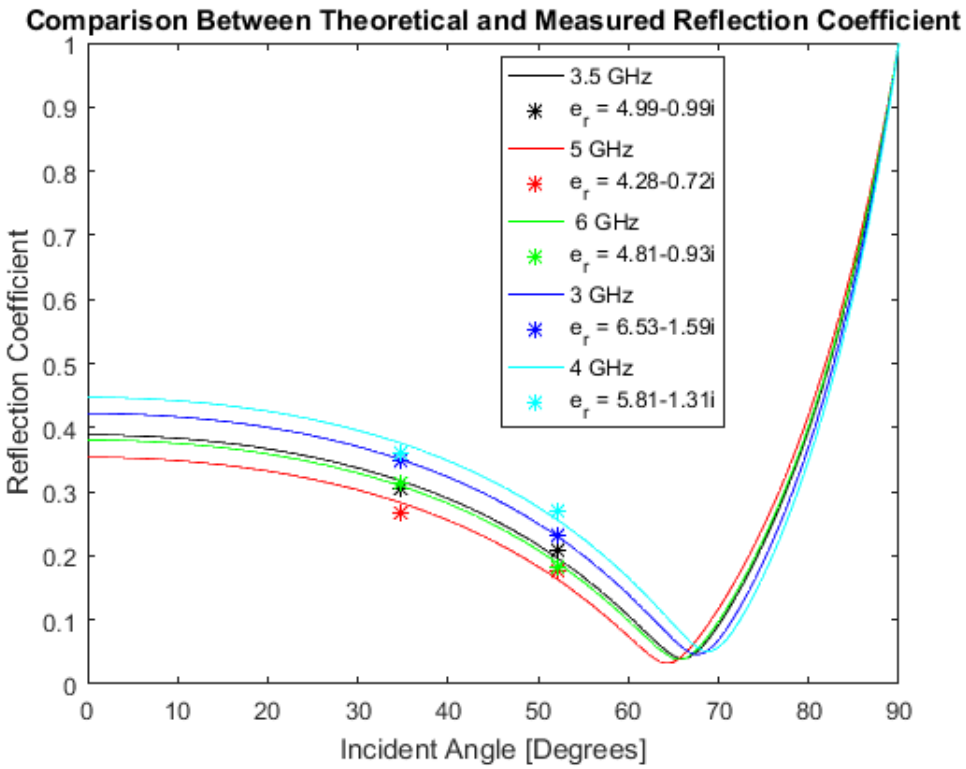

Figure 31. Theoretical vs Measured (Parallel)

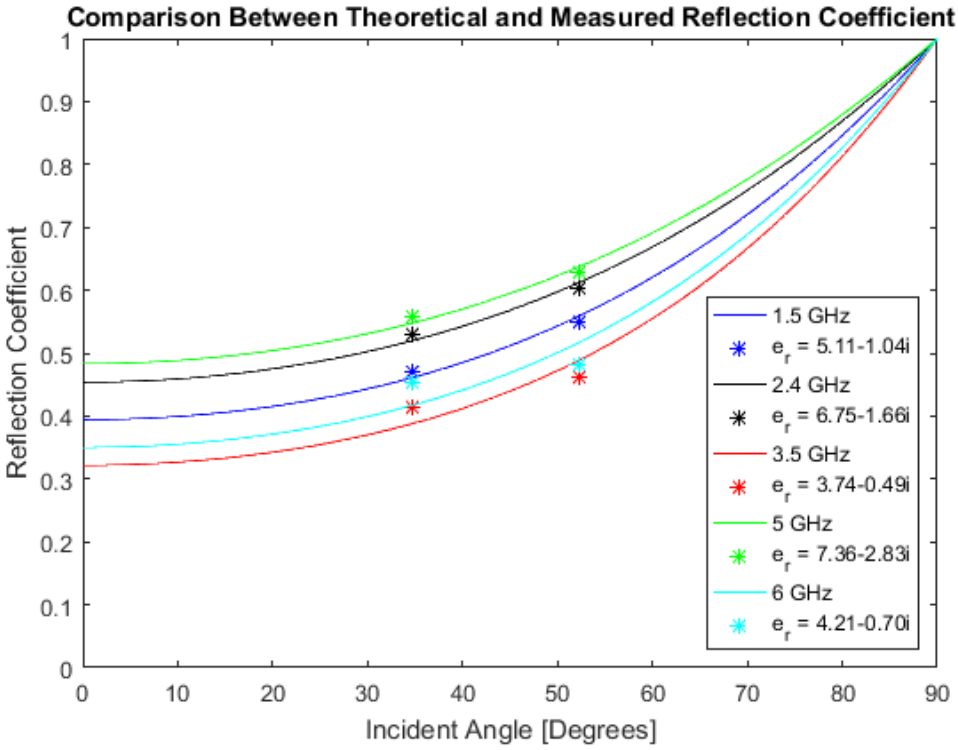

Figure 32. Theoretical Vs Measured (Perpendicular)

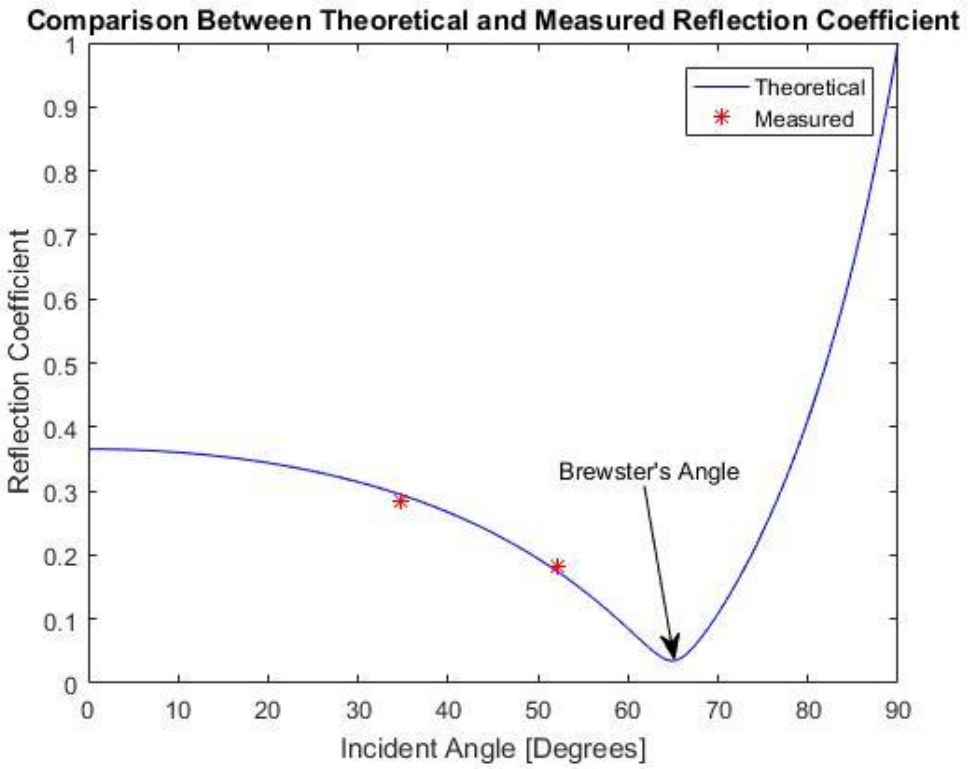

Figure 33. Brewster's Angle Representation

4.6.2. Indoor Concrete Wall

The complex relative permittivity for indoor wall was estimated using the algorithm mentioned in the previous sections. Reflections from three incident angles were used to reconstruct the theoretical reflection coefficient by estimating the value of ε_r. The concrete wall was inside an enclosed corridor, and is assumed dry. The thickness of the measured wall was 0.136 m. The measured reflection coefficients were calculated using equation (4.2). Firstly, the permittivity was calculated for the frequency range of 2.5-6 GHz, where the antenna responses were best and least errors were expected. The estimated complex relative permittivity for parallel polarization in this case is 3.2426-0.7567i and 2.9435-0.6412i for perpendicular polarization. The loss tangent values for both polarizations are 0.2334 and 0.2178, respectively. However, the presentation of theoretical and measured values of reflection coefficients could not be explained precisely for this approach. Hence, ε_r was estimated at several frequency points and the comparison between theoretical and measured values are mentioned in Figure 34 and 35. The reflected signal strength for both polarizations varied significantly for all incident angles. This explains both polarizations are at good agreement. The thickness of the wall is significant compared to the wavelength, therefore no errors are considered due to wavelength of the wave for the chosen frequency range. The algorithm minimized the differences between the measured and theoretical values estimated the aforementioned values of ε_r. Measurement at a single point is sufficient for the extract of permittivity profiles of a material. However, a larger number of incident angles give more accurate estimation of permittivity profiles. Therefore, the measurements were repeated for several points to estimate the error of ε_r, which will be discussed in this

chapter. The measured and theoretical reflection coefficients for both polarizations for the chosen frequency range are compared in Figures 34 and 35.

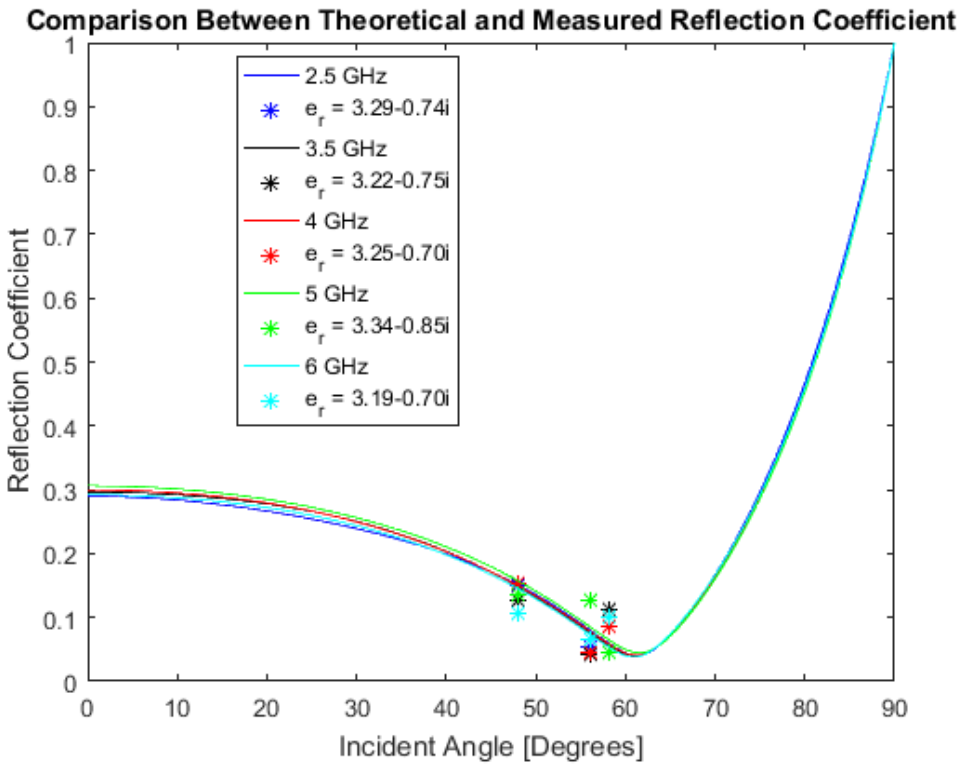

Figure 34. Measured Vs Theoretical (Parallel)

It can be seen from the figures, the measured and theoretical values give good agreement with the estimated value of ε_r. Therefore, the theoretical reflection coefficient does not fluctuate as much as the measured values and seems to be constant over the frequency range. Since, ε_r is the function of frequency, the theoretical reflection coefficient in perpendicular polarization does not completely follow the measured value at all frequencies. It can be due to inhomogeneity of wall and the influence of other materials within the wall.

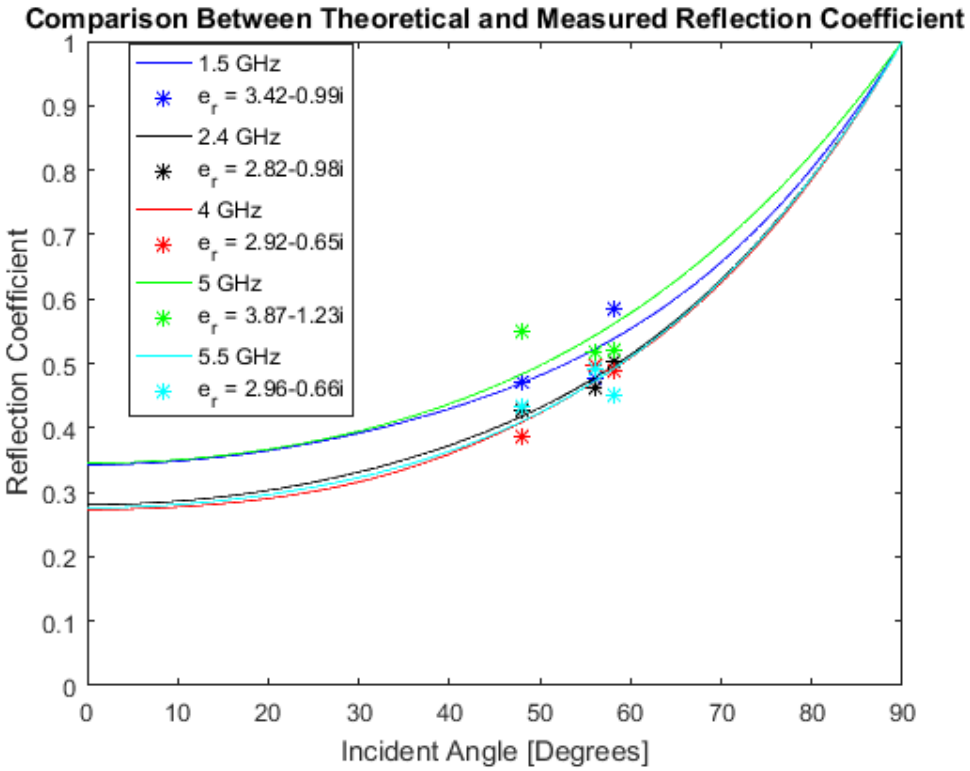

Figure 35. Measured Vs Theoretical (Perpendicular)

The measurements for the indoor concrete wall were repeated for different incident angles. The measurement setup and the scenario were explained in section 4.4.2. The behavior of reflection coefficient in this case clearly shows that better prediction of the dielectric properties of a material is achieved by measuring a larger number of points. Results with a wide range of incident angles agreed reasonably with the behavior of the electromagnetic waves on interaction with the dielectric boundary. The estimated values of complex permittivity for both polarizations were 3.4696-0.9557i and 3.0291-0.7082i, respectively. The comparison between the measured and theoretical values of reflection coefficient with the estimated ε_r is shown in Figure 36 and Figure 37. Measurement at larger number of incident angles enabled to get more stable results compared to all the other scenarios. Thus, real and imaginary part of ε_r is shown in Figure 38 and 39 as a function of frequency.

From Figures 34 to 37, the difference in the estimated values of dielectric constant is observed to be ± 0.6 for both the polarizations. The values of reflection coefficient in the first and second measurement cases differ near the same angles due to the asymmetry of the measurement of distances during the measurements for first case. Hence, the perpendicular polarization values for ε_r is also sensitive to the number of angles and the symmetry of the experiment. The error analysis using these measurements is done later in this chapter. The Brewster's angle was calculated to be 62.01° is shown in Figure 40 for a single frequency for simplicity.

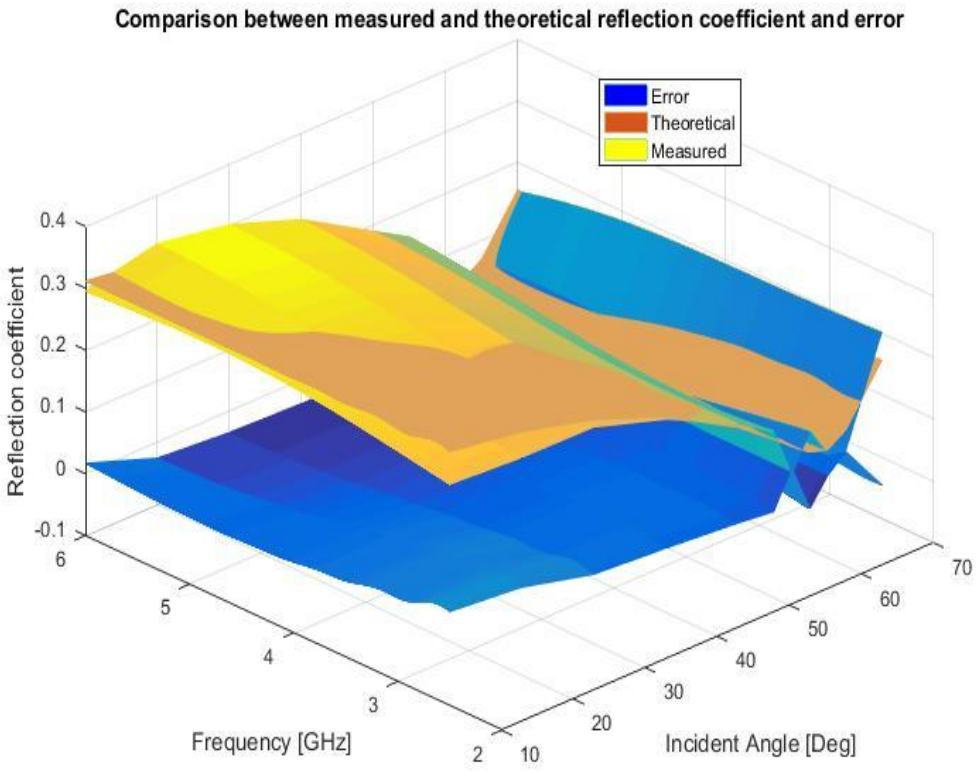

Figure 36. Theoretical Vs Measured (Parallel)

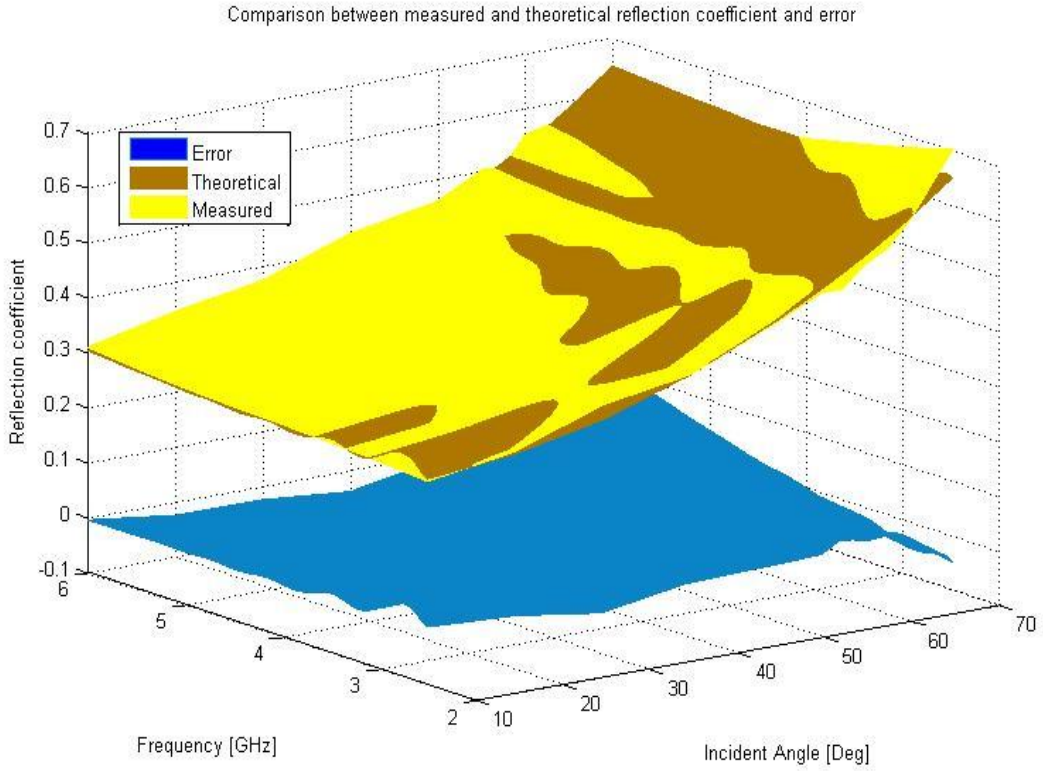

Figure 37. Theoretical Vs Measured (Perpendicular)

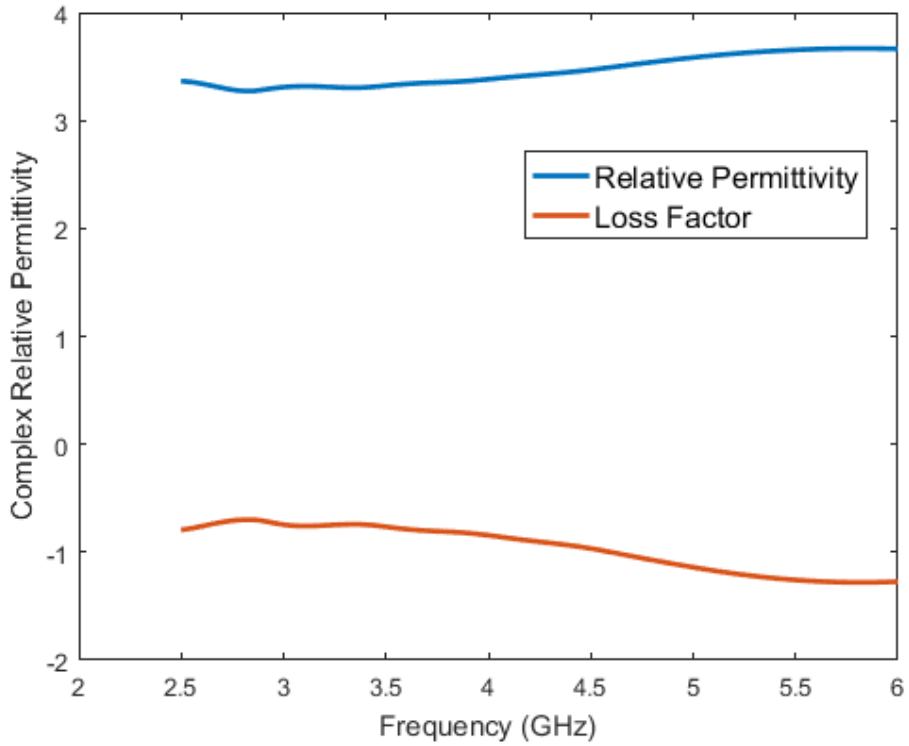

Figure 38. Complex Relative Permittivity Vs Frequency (Parallel)

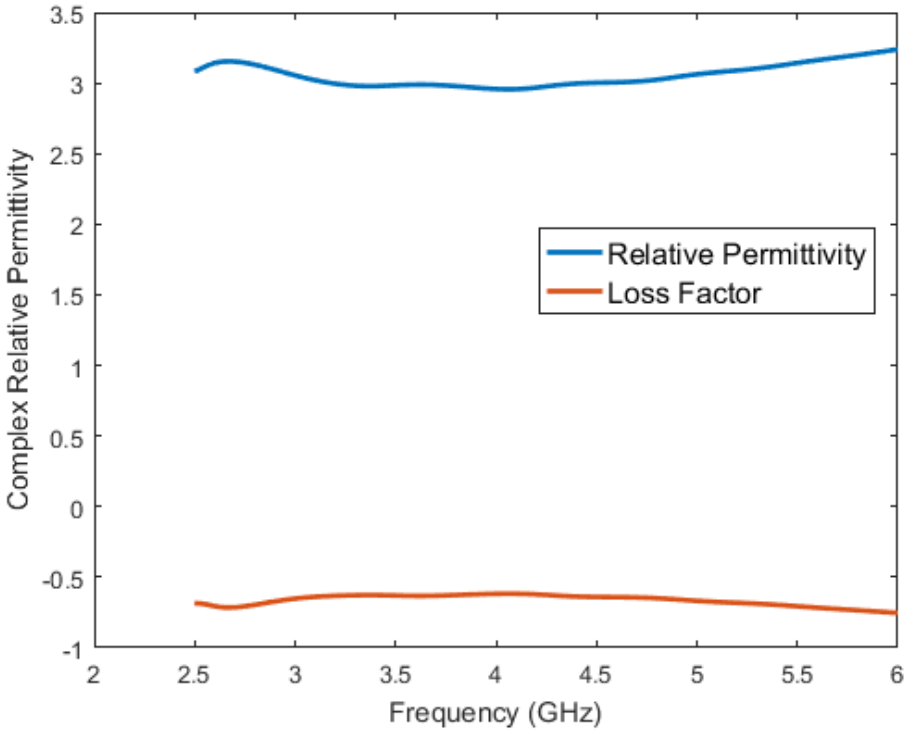

Figure 39. Complex Relative Permittivity Vs Frequency (Perpendicular)

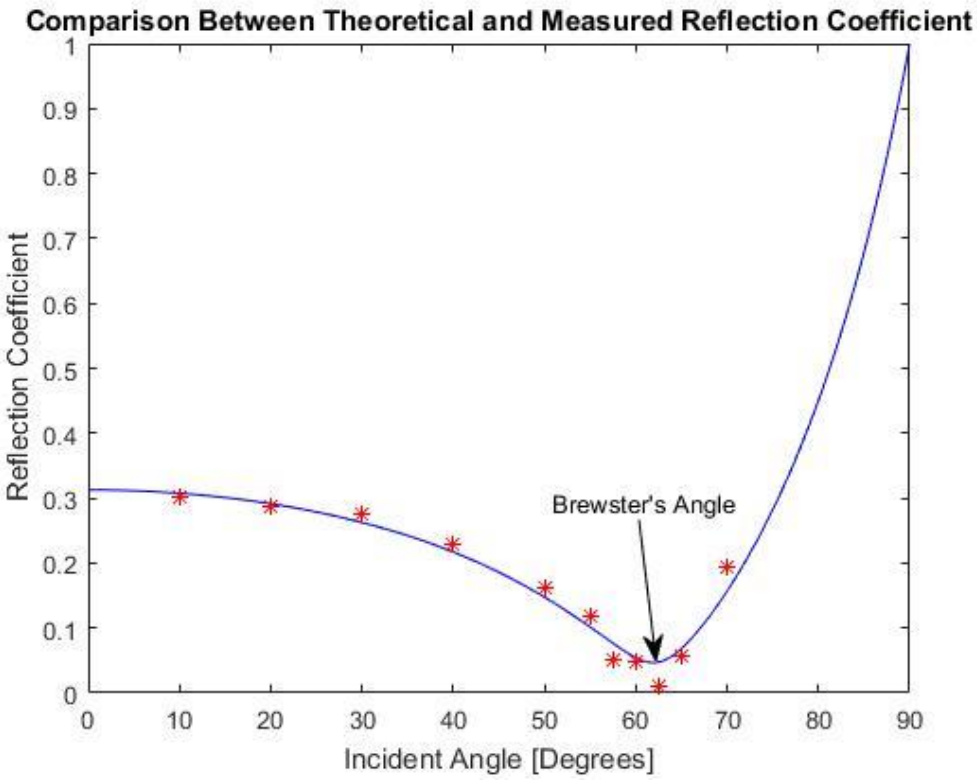

Figure 40. Brewster's Angle Representation

4.6.3. Indoor Classroom Brick Wall

Measurements were performed at four different angles of incidence for the estimation of dielectric constant of a porous brick wall with foam type material behind the bricks. The reflection characteristics of the wall are presented in Figures 24 and 25. It is clear from the figure that very low power was received at all incident angle. The measured reflection coefficients for parallel and perpendicular polarizations varied significantly over the entire frequency range for all incident angles, 12.44°, 34.41°, 40° and 54° respectively. The nature of the bricks and the foam type absorbing material resulted in very low reflection coefficient values, which can also introduce errors in the frequency response data. It is suspected that the incident waves were absorbed by the porous surface and the foam type material. Large number of holes in the brick allowed direct contact between the absorbing material and incident electromagnetic waves, which can explain the significant attenuation in the received signal. The worst case was recorded for 12.44°, for which the recorded value of reflection coefficient is lowest. At this angle, errors can occur due to coupling between the antennas as both the antennas come very close to each other [6] but it was verified that there did not exist any coupling between the antennas at smaller incident angles. It can be seen from Figures 24 and 25 that, the roughness of the wall has resulted in highly distorted received signal. It was very difficult to find the reflected wave in delay analysis, the holes on the bricks can lead to unexpected scattering of the incident waves in any direction. However, at higher incident angle, i.e. in the fourth measured scenario in this case, the holes are nearly invisible to the electromagnetic waves and assuming the surface being smooth. Thus, at this incident angle, the reflected wave was clearly visible on the delay plot. However, time domain gating was applied to clearly separate the reflection from the point of

interested for all cases. The fluctuations in the frequency response data did not allow a good visualization of trend of reflection coefficient over the frequency range for the estimated ε_r. Therefore, the estimation of dielectric constant is done at several frequency point within the measured frequency range. The estimated value of dielectric constant for this case is shown in Figure 41 and 42 for parallel and perpendicular polarization, respectively. The low value of dielectric constant is due to the absorbing material behind the bricks. The estimated permittivity value seems to be constant for chosen frequency points.

The nature of the brick and absorbing foam has resulted in very small reflection coefficient which is almost the same in both the cases. Brewster angle is present at 49.09° in the theoretical model plot for parallel polatization which can be seen from Figure 41. At this point the absolute value of reflection coefficient is minimum. The theoretical reflection coefficient response shows several variation at different angles. It is the result of rough surface of the wall. However, the theoretical values are at good agreement with the measured values of reflection coefficient and permittivity values are almost constant at all frequencies.

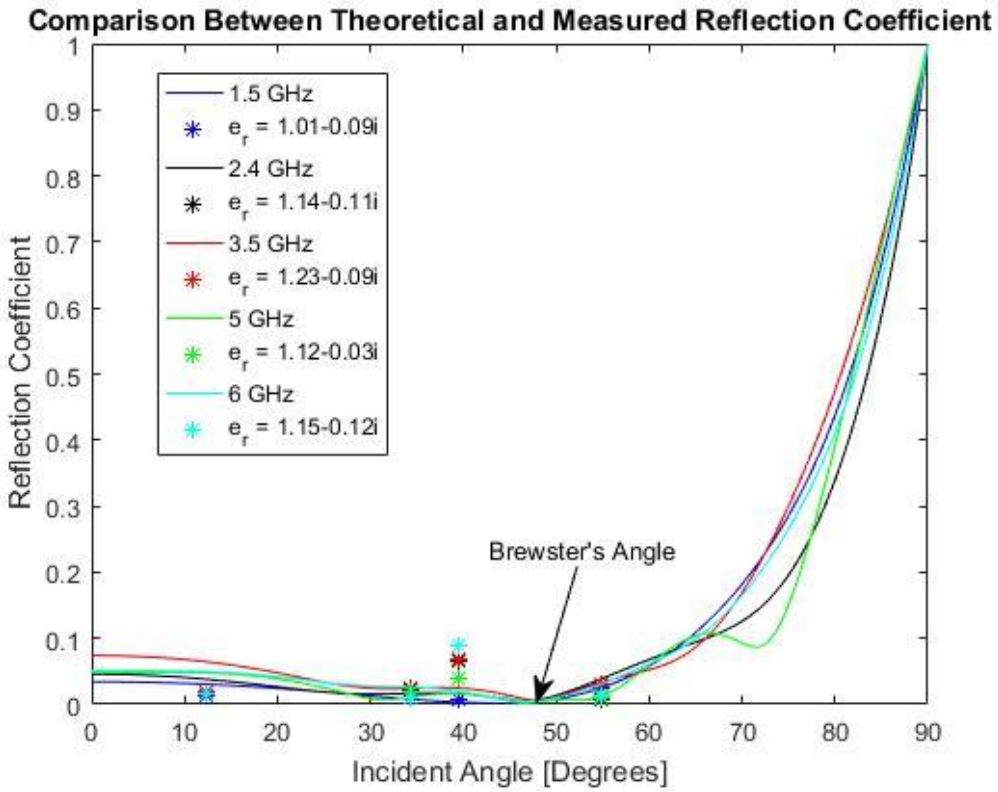

Figure 41. Theoretical Vs Measured (Parallel)

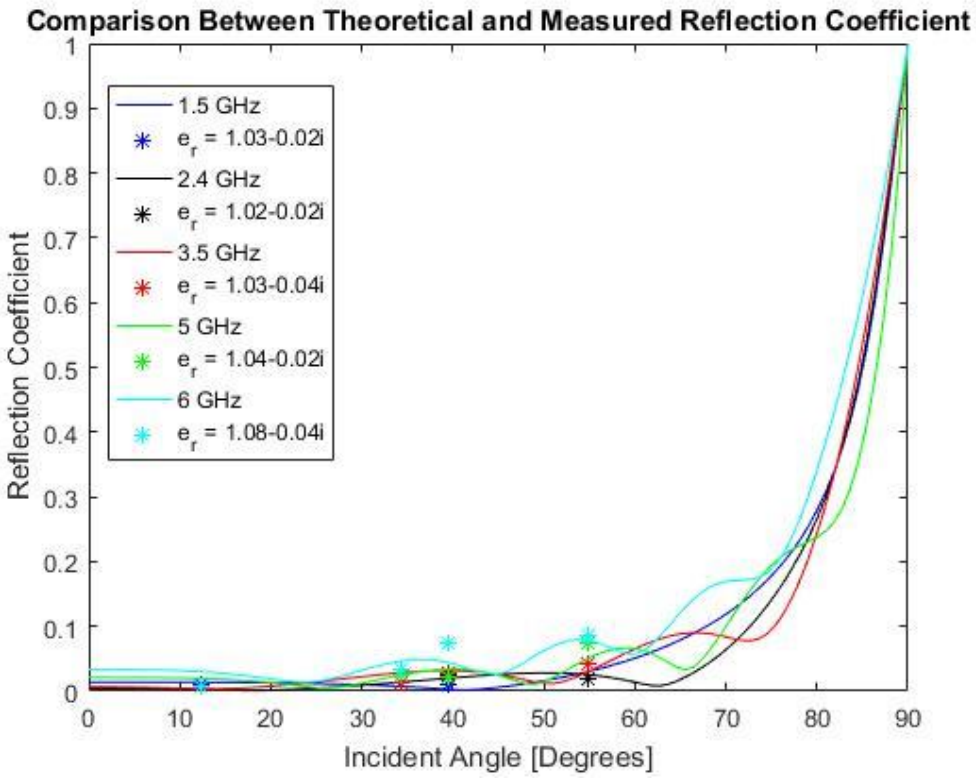

Figure 42. Theoretical Vs Measured (Perpendicular)

4.6.4. Painted Brick Wall

The dielectric properties for a painted wall were extracted using the reflected fields at various incident angles. The absolute value of the reflection coefficient was measured for both polarizations. The measured responses contained unknown reflected peaks. These unwanted peaks in the responses have been shown in Figure 29 and 30. The absolute values of measured reflection coefficients for both polarizations were extracted from 2.5-6 GHz for incident angles 38.18°, 70.28°, 74.27°, respectively. Fitting the reflection coefficient to the measured value does not give a good understanding for both polarization due to the unknown reflections that may be contributing to the interested reflection from behind the wall. The estimated values of dielectric constant for parallel polarization is 4.5297-0.5837i. The comparison of measured and theoretical reflection coefficient is shown in Figure 43 for parallel polarization at several discrete frequency points. The fitting is satisfactory only at lower frequencies as can be seen in Figure 43. Several error were expected for this measurement. Thus unrealistic theoretical reflection coefficient at 4 and 5 GHz can be the result of unexpected error in the measurement data. The Brewster angle in this case can be seen in Figure 44 at 64.41°. The reflection coefficient at this angle is close to zero. The Brewster's angle here is shown at only one frequency for simplicity. The estimated value of dielectric constant are not in good agreement for all the frequencies according the characteristics of the reflection coefficients. The internal structure and contributions from unknown materials may have introduced inseparable errors in the recorded responses. Therefore, the theoretical reflection coefficient shows a constant behavior over all the frequencies due to constant ε_r value over the frequency range. If the medium was homogeneous and the responses contain minimum error, then the theoretical reflection coefficient should follow the

measured values at all frequencies. As, the value of ε_r does not vary significantly over the frequency range for same material. The nature of the paint has also influenced the reflection characteristics in this case that as a result will affect the permittivity profile of the MUT. In case of perpendicular polarization, the behavior of reflection coefficients at large angles is contradicting from the expected behavior. Therefore, large errors due in the data did not allow the estimation of dielectric properties in case of perpendicular polarization. It is suspected to be the effect of some metal structure or reflection from the surface behind the medium or other unwanted signal interfering with the signal of interest, which has led to catastrophic errors in the data. These irregularities can be overcome and verified by adding more points in the measurement data and more precise measurement setup.

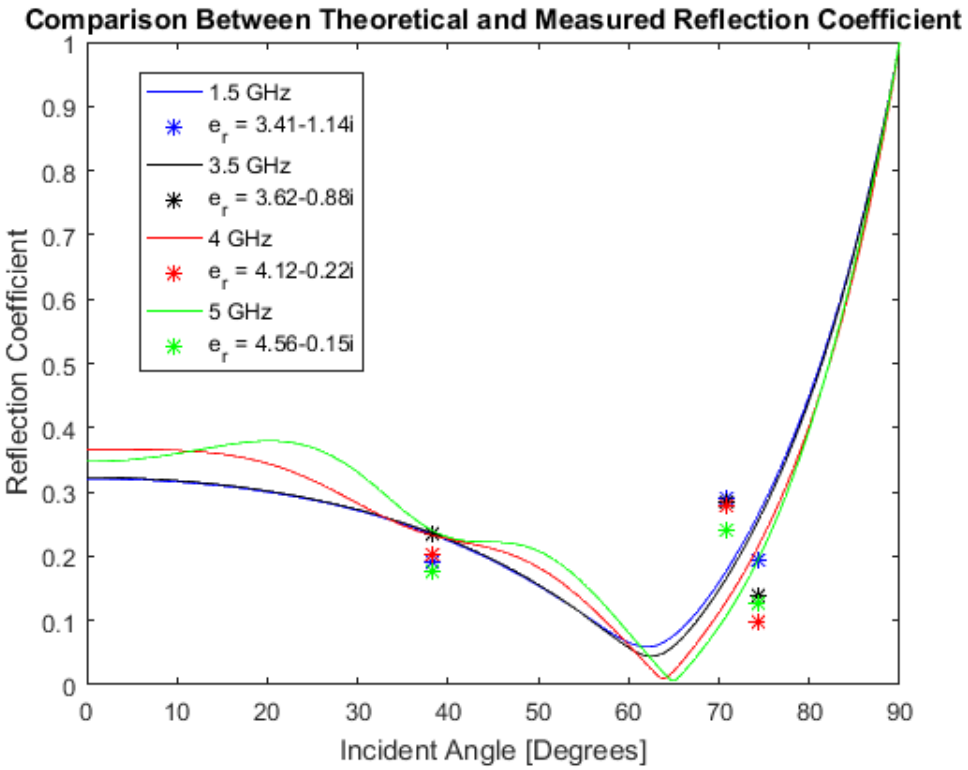

Figure 43. Theoretical Vs Measured (Parallel)

Figure 41, shows a very different response of reflection coefficient. It is mainly due to less number of measurement points, significant difference between the first and the second measured point and some errors due to unknown responses captured from behind the wall or from the surroundings. Although the estimate of dielectric constant will not be affected significantly for this measurement, to get the proper behavior of reflection more number of incident angles have to be investigated.

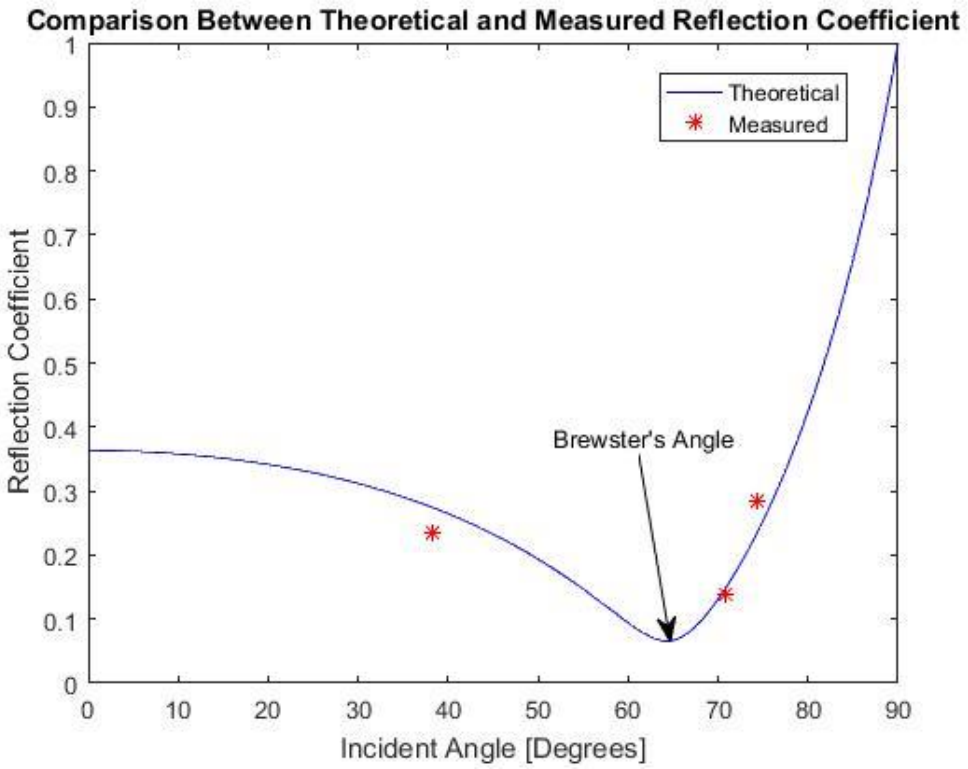

Figure 44. Brewster's Angle Representation

Dielectric properties of different building walls were discussed. Different building materials showed different behavior on interaction with electromagnetic waves that is determined by the permittivity of the medium. The Brewster angle was determined by the theoretical reflection model for the aforementioned scenarios. The error analysis and the tabulated values of the dielectric constant, loss tangent, reference values and the mean squared error between the measured and the theoretical reflection coefficient values are presented in the next section.

4.7. Error Analysis

Measured responses are very prone to errors from noise generated by the devices, multiple reflections from the surroundings, dimension errors, harsh environments and heterogeneity of MUT, etc. Therefore, error analysis is the key factor in the investigation of measured responses. The errors in the measured dimensions were ± 0.01 m to ± 0.04 m that can lead to errors in the measured incident angles up to $\pm 0.5°$ which was considered insignificant. The other sources of errors were the internal structure of the walls that may contain several other materials that are very difficult of separate out. There are also air gaps present inside the structure of the wall, that introduce errors in the measurement data.

The error between the measured and theoretical values of reflection coefficient was estimated by the root mean-squared error of the error function given by equation (4.9).

$$rmse = \frac{1}{(N-1)(T-1)} \sqrt{\sum_{t=1}^{T} \sum_{i=1}^{N} \left| \Gamma_{\mathrm{tot_{thy}}}(\theta_i, f_t) - \Gamma_{\mathrm{meas}}(\theta_i, f_t) \right|^2} \tag{4.9}$$

Here, *N* is the number of incident angles; *T* is the number of samples [1]. The dielectric properties and mean-squared error are presented in Table 3 and Table 4 for parallel and perpendicular polarization, respectively. Since the estimate of complex permittivity is an approximation process, some errors are always present in the calculated value due to the aforementioned reasons. Therefore, an algorithm that gives the lower value of rmse, is supposed to give better approximation for the permittivity values. However, the algorithm used to optimize the objective function tends to find better minimum for less number of measurement points because it is easy to fit less number of points. Thus, using only the root mean-squared error of the objective function is not a completely reliable method to predict error for dielectric constant. However, repeated measurements at different angles of incidence can give a good agreement for the estimation of ε_r and give better estimate of error. The errors between measured and theoretical reflection coefficients were plotted in section 4.6 for all the measurement scenarios as a function of frequency and incident angles. The measurements with twelve-measured angle of incidences give the best result as compared to all the other cases. The differences in the values in case of indoor concrete wall are the results of mismatch in dimensions between the two measurements and due to inaccuracies due to less number of measurement points in one scenario. Thus, from Figure 36 and 37, better approximation is achieved with more number of incidence angles. However, in all the cases, errors were greater near the Brewster's angle and beyond as compared to smaller incident angles. Errors can occur near Brewster angle due to the very low value of reflection coefficient. Inaccuracies during the measurement of incident angles can cause significant differences in the estimated dielectric constant values. A better estimation of loss factor can be achieved by gaining the complete knowledge of the internal structure of the MUT, which contribute to the losses in the received signal. It is observed that loss factor is larger in case of parallel polarization due to better penetrating capability of the parallel-polarized wave.

The estimated values of dielectric properties of investigated materials are compared with the values found in various scientific publications, and are presented in Table 3 and Table 4. The dielectric constant values agree well with the results published in various scientific papers. However, there is less certainty of accuracy of the loss factor or the loss tangent. The uncertainty in the loss tangent depends on the material composition, measurement accuracy. The values presented in this thesis, agree well for the mentioned materials, and hence can be used for further scientific purpose. The error analysis for indoor concrete wall can be used to elaborate the trend of errors that would have influenced the permittivity values in other scenarios as well. The complex permittivity compared between different literatures also does not give exact same values. Therefore, an approximately closer value can be used for desired purpose. Hence, it can be concluded that the approximation of the permittivity can be used in radio propagation design by investigating a range of permittivity values that satisfy the corresponding scenario.

This thesis follows a typical ray optics model for electromagnetic propagation, as shown in Figure 9. Here, the transmitted and reflected radio waves considered a ray and not a beam with certain beamwidth. The beamwidth depends on the frequency and the

type of antenna used. The beamwidth decreases with increase in frequency. Thus, thesis does not take into account the varying beam-footprint over the frequency range on the reflected surface, which could affect the signal analysis and the accuracy of the measured data. In addition, the more accurate analysis of internally reflected signals will lead to result that is more accurate. The rough estimate of internally reflected waves was carried out during the signal analysis. The gate applied during the measurement for smaller incident angles captured the first internally reflected signal. However, at larger incident angles highly attenuated internal reflections were analyzed that did not have any effect on the recorded data.

The measurement setup, scenarios and results were discussed in this chapter. In the next section, the discussions and suggestions regarding the study along with some improvements in the measurement system will be discussed briefly.

Table 3: Building Walls Electromagnetic Properties for Parallel Polarization

Building Walls	Dielectric Constant	Loss Tangent	Reference Value [Dielectric Constant]	Reference Value [Loss Tangent]	Brewster Angle	Root Mean Squared Error (rmse) of Γ
Outdoor Concrete Wall	5.1437	0.2051	3-15 [3]	0.04-1.2 [33]	65.02°	$2.5e^{-3}$
Indoor Concrete Wall(3points)	3.2426	0.2334	3.1726 [6]	0.0184 [6]	-	$1.9e^{-3}$
Indoor Concrete Wall(12points)	3.4696	0.2754	3.1726 [6]	0.0184 [6]	62.01°	$2.7e^{-4}$
Classroom Absorber Brick Wall	1.1735	0.0261	1.11 [34]	-	49.09°	$1e^{-3}$
Painted Brick Wall	3.5607	0.0157	3.88-4.26 [35]	0.1173-0.1209 [35]	64.41°	

Table 4: Building Walls Electromagnetic Properties for Perpendicular Polarization

Building Walls	Dielectric Constant	Loss Tangent	Reference Value [Dielectric Constant]	Reference Value [Loss Tangent]	Root Mean Squared Error (rmse)
Outdoor Concrete Wall	5.7663	0.1615	3-15 [3]	0.04-1.2 [33]	$6e^{-3}$
Indoor Concrete Wall(3points)	2.9435	0.2178	2.77 [7]	0.0069 [7]	$3.5e^{-3}$
Indoor Concrete Wall(12points)	3.0291	0.2338	3.2582 [6]	0.0259 [6]	$2.6e^{-4}$
Classroom Absorber Brick Wall	1.0121	0.0582	1.11 [34]	-	$8.4e^{-4}$

5. DISCUSSION

The reflection measurements of different building walls were performed at several angles of incidence over the frequency range of 0.7-7 GHz. The measurement system was able to perform efficiently for the proposed objective of the study. However, several improvements can be done in future to adapt more accurate measurement system to study the reflection characteristics of building materials. Efficient planning before the measurement could be very crucial for the accuracy of the measurement. Some of the improvements in the measurement system and future work are discussed further.

5.1. Improvements in the Proposed Measurement System

The measurement system gave good agreement of the extracted values of electromagnetic properties of building walls, however many improvements and additional measurement scenarios can enhance the accuracy of results in the future. The surroundings during the time measurement were congested by people walking around. The measurements were performed in an enclosed boundary to avoid traffic from disturbing the measurements setup, and thus the environment did not affect the experiment. WLAN and cellular signal at the university were not considered to contribute to the received data. Wideband dual-polarized cross-shaped Vivaldi antennas were used for the measurement. The antenna gains were in the range of 3.8-11.2 dB. Higher-gain antennas can be used to receive higher power after reflection. The beamwidth of antenna varied along the frequency range. Therefore, implementation of ray model is better with narrower beamwidth. Some of the cases in this study showed very small-received power, which indicates small reflection coefficient, and at very small received, power levels errors are easily introduced in the signal. The use of dual-polarized antennas enabled to take simultaneous measurements for both polarizations without changing the position of the antenna after every recording (single polarized antenna should be rotated by 90° to capture both polarizations). However, cross-polarization and co-polarization components may still interfere with the responses. The cross-polarization discrimination of the antennas was above 19 dB, and therefore the cross and co-polarizations interference was not considered in this study. The model used for this study considers the walls to be homogeneous, but there are certainly few layers of other materials present within the walls. Therefore, complete knowledge of the walls i.e. the exact materials used and the layers within the wall could be investigated in detail for future experiments.

The number of measurement points, or the number of incident angles, for all scenarios were from two to four. A measurement with twelve points was conducted for verification of the experiment. For more accurate behavior of reflections from different dielectric surfaces, a larger number of symmetrically spaced incident angles should be considered. These angles may also include the Brewster angle, hence it would be more efficient to also compare the measured and theoretical values of Brewster angle. This study only concentrated on one internal reflection from the material, but proper analysis during the measurement and separation of all the internally reflected signals by applying a better gating will allow better estimation and reduce the uncertainty of estimated results.

5.2. Future Works

The estimation of dielectric properties of different building walls was performed over 0.7-7 GHz frequency range. The heterogeneity of walls was not considered by the used model. Dielectric properties for different layers of the structure can be calculated and a different theoretical model can be proposed for future experiments regarding this study. A time domain approach was used in this study. The frequency dependency of the dielectric constant can be determined by repeating the experiments for more frequency points and the knowledge of internal structure of the MUT. With the advancement in communication technologies, future frequency bands should be investigated for designing efficient propagation models. Thus, this study is very essential in designing radio propagation model for complex buildings, especially in cold countries such as Finland where buildings consists of several layers of construction materials.

6. SUMMARY

The main objective of this thesis was to extract the dielectric properties of building walls 0.7-7 GHz frequency band. A suitable measurement setup was proposed, which included two wideband dual-polarized cross-shaped Vivaldi antennas, a VNA, and coaxial cables. The setup was very simple for implementation. However, to measure the incident angles accurately, the measurements were very lengthy due to adjustments of the distance between the antennas and walls. Two test measurements were performed in the anechoic chamber, one for the LOS measurement and the other for the measurement of reflection from the metallic floor. These measurements were necessary to check the responses of different antennas, so that they do not differ to each other significantly and the responses were necessary to calculate the reflection coefficient by normalizing the measured value of received signal strength by the received signal strength of the test measurements.

Reflection measurements for four different types of walls were performed that consisted of an outdoor concrete wall, an indoor concrete wall, a brick wall containing holes and absorbing foam inside the structure, and a painted brick wall. Time domain gating was used to eliminate multiple reflections from the surroundings and the LOS component. The incident angles were randomly chosen for all cases. A theoretical reflection model was used to extract the dielectric properties of various building walls. The measured and the theoretical reflection coefficients were functions of incident angles and frequency. The non-linear least squares algorithm was used to find the minimum of the objective function which was the minimum difference between the theoretical and measured absolute value of reflection coefficient for the best possible permittivity values. The absolute value of reflection coefficient was plotted from 0 to 90°, for parallel polarization at a single frequency to visualize the Brewster's angle, given by the theoretical model. The walls gave a good estimate of complex relative permittivity i.e., the dielectric constant as well as loss factor. However, the uncertainty in the loss factor is very difficult to analyze and accurate value is never achieved. The estimated values were also compared to the estimated values in several scientific publications. Error analysis was done using the responses of the repeated measurements for indoor concrete wall. Several values of permittivity have been compared with the previous measurement outcomes to estimate the errors in permittivity. It was concluded that measurement at several angles give better estimate of dielectric properties of a material and can completely determine the reflection behavior from the theoretical model. However, measurement at fewer points considerably gives good results that can be used for design purpose but it cannot predict the reflection behavior of radio waves correctly. The theoretical model also gave the value of Brewster angle for all the cases, which can be used for further channel modelling purposes. These values can be used to predict the reflection and transmission characteristics of the building materials, as they are the key features to forecast the electromagnetic propagation phenomenon through and from the building walls.

7. REFERENCES

[1] I. Vilovic, N. Burum and R. Nadj, "Estimation of dielectric constant of composite materials in buildings using reflected fields and PSO algorithm," *Proceedings of the Fourth European Conference on Antennas and Propagation*, Barcelona, Spain, 2010, pp. 1-5.

[2] Huang, Y.; Nakhkash, M., "Characterisation of layered dielectric medium using reflection coefficient," in *Electronics Letters*, vol.34, no.12, pp.1207-1208, 11 Jun 1998.

[3] Hong, C. Rhim; Oral Buyukozturk, "Electromagnetic Properties of Concrete at Microwave Frequency Range," in *Material Journal,* vol.95, no.3, pp.262-271, 5 Jan 1998.

[4] Rodriguez, I.; Nguyen, H.C.; Jorgensen, N.T.K.; Sorensen, T.B.; Mogensen, P., "Radio Propagation into Modern Buildings: Attenuation Measurements in the Range from 800 MHz to 18 GHz," in *Vehicular Technology Conference (VTC Fall), 2014 IEEE 80th*, vol., no., pp.1-5, 14-17 Sept. 2014

[5] Ghodgaonkar, D.K.; Varadan, V.V.; Varadan, Vijay K., "A free-space method for measurement of dielectric constants and loss tangents at microwave frequencies," in *Instrumentation and Measurement, IEEE Transactions*, vol.38, no.3, pp.789-793, Jun 1989

[6] I. Vilovic, R. Nad, Z. Sipus and N. Burum, "A non-destructive approach for extracting the complex dielectric constant of the walls in building," *ELMAR, 2008. 50th International Symposium*, Zadar, 2008, pp. 609-612.

[7] Lu, Jonathan, Daniel Steinbach, Patrick Cabrol, Phil Pietraski, and Ravikumar V. Pragada. "Propagation characterization of an office building in the 60 GHz band." In *The 8th European Conference on Antennas and Propagation (EuCAP 2014)*, pp. 809-813. IEEE, 2014.

[8] L. M. Correia and P. O. Frances, "Estimation of materials characteristics from power measurements at 60 GHz," *Personal, Indoor and Mobile Radio Communications, 1994. Wireless Networks - Catching the Mobile Future., 5th IEEE International Symposium on*, The Hague, 1994, pp. 510-513 vol.2.

[9] J. Ahmadi-Shokouh, S. Noghanian, E. Hossain, M. Ostadrahimi and J. Dietrich, "Reflection Coefficient Measurement for House Flooring Materials at 57-64 GHz," *Global Telecommunications Conference, 2009. GLOBECOM 2009. IEEE*, Honolulu, HI, 2009, pp. 1-6.

[10] Räisänen, Antti V., and Arto Lehto. *Radio Engineering for Wireless Communication and Sensor Applications*. Boston, MA: Artech House, 2003.

[11] Balanis C.A. (2005) *Antenna Theory - Analysis and Design*. JohnWiley & Sons, third ed.

[12] Pozar, David M. *Microwave Engineering*. Hoboken, NJ: J. Wiley, 2005, third ed.

[13] Bevelacqua, Pete. "The Antenna Theory Website". http://www.antenna-theory.com/ . N.p., 2016. Web. 6 June 2016.

[14] Collin, Robert E. *Antennas and Radiowave Propagation*. New York: McGraw-Hill, 1985

[15] Fleisch D. (2008) A Student's Guide to Maxwell's Equations. Cambridge University.

[16] Inan, Umran S and Aziz S Inan. *Electromagnetic Waves*. Upper Saddle River, N.J.: Prentice Hall, 2000.

[17] Tervo N. (2014) Virtual Antenna Array Based MIMO Radio Channel Measurement System at 10 GHz. University of Oulu, Department of Communications Engineering, Degree Programme in Electrical Engineering. Master's Thesis, 58 p.

[18] Y. Huang, and M. Nakhkash, "Characterization of Layered Dielectric Medium Using Reflection Coefficient", *Electronic Letters,* Vol. 34, No. 12, pp.1207-1208, 1998.

[19] Introduction to Network Analyzer Measurements *Fundamentals and Background,* RF Academy – National Instruments, Web. 15 June 2016. http://download.ni.com/evaluation/rf/Introduction_to_Network_Analyzer_Measurements.pdf

[20] Chen, L.F. et al. *Microwave Electronics: Measurement and Materials Characterization*. Wiley, 2004. Print.

[21] Editor, The. "Microwaves101 | S-Parameters", Web. 15 June 2016. https://www.microwaves101.com/encyclopedias/438-s-parameters-microwave-encyclopedia-microwaves101-com

[22] Agilent Time Domain Analysis Using a Network Analyzer, Application Note 1287-12, http://cp.literature.agilent.com/litweb/pdf/5989-5723EN.pdf

[23] Time Domain Measurements using Vector Network Analyzer ZVR, Application Note 1EZ44_0E, May 1998 https://cdn.rohde-schwarz.com/pws/dl_downloads/dl_application/application_notes/1ez44/1ez44_0e.pdf

[24] "Windowing", Web. 27 June 2016. http://www.cs.tut.fi/kurssit/SGN-4010/ikkunointi_en.pdf

[25] "FIR Design by Windowing, Kaiser Window and Optimal Approximation", University of Washington, Dept. of Electrical Engineering, November 28, 2001. http://melodi.ee.washington.edu/courses/ee518/notes/lec17.pdf

[26] "Measurement Errors". Web, 29 June 2016 http://na.support.keysight.com/pna/help/latest/S3_Cals/Errors.htm

[27] Khan, Muhammad Talha, and Syed Muzamil Ali. "A brief review of measuring techniques for characterization of dielectric materials." *International Journal of Information Technology and Electrical Engineering* 1.1 (2012).

[28] Keysight Technologies, Keysight 2-Port and 4-Port PNA-X Network Analyzer N5247A - 10 MHz to 67 GHz, "Data Sheet and Technical Specifications". Web 7 July,2016, http://literature.cdn.keysight.com/litweb/pdf/N5247-90002.pdf?id=1994005

[29] M. Sonkki, D. Sánchez-Escuderos, V. Hovinen, E. T. Salonen and M. Ferrando-Bataller, "Wideband Dual-Polarized Cross-Shaped Vivaldi Antenna," in *IEEE Transactions on Antennas and Propagation*, vol. 63, no. 6, pp. 2813-2819, June 2015.

[30] O. Landron, M. J. Feuerstein and T. S. Rappaport, "A comparison of theoretical and empirical reflection coefficients for typical exterior wall surfaces in a mobile radio environment," in *IEEE Transactions on Antennas and Propagation*, vol. 44, no. 3, pp. 341-351, Mar 1996.

[31] https://se.mathworks.com/help/optim/ug/lsqnonlin.html

[32] J. Joseph, R. Jost and E. Utt, "Mutiple angle of incidence measurement technique for the permittivity and permeability of lossy materials at millimeter wavelengths," *Antennas and Propagation Society International Symposium, 1987*, Blacksburg, VA, USA, 1987, pp. 640-643.

[33] Stavrou, S., and S. R. Saunders. "Review of constitutive parameters of building materials." *Antennas and Propagation, 2003. (ICAP 2003). Twelfth International Conference on (Conf. Publ. No. 491)*. Vol. 1. IET, 2003.

[34] A. Safaai-Jazi, S.M. Riad, Ali Muqaibel, and A.Bayram, *"Report on Through-the-Wall Propagation and Material Characterization",* Time Domain and RF Measurement Laboratory, Bradly Department of Electrical Engineering, Virginia Polytechnic Institute and State University, Blacksburg, Virginia, November, 2002.

[35] C. A. Grosvenor, R. T. Johnk, J. Baker-Jarvis, M. D. Janezic and B. Riddle, "Time-Domain Free-Field Measurements of the Relative Permittivity of Building Materials," in *IEEE Transactions on Instrumentation and Measurement*, vol. 58, no. 7, pp. 2275-2282, July 2009.

8. APPENDIX

Flowchart for the Estimation of Dielectric Properties of Various Materials